การสร้างแบบจำลองเชิงโมเลกุลของสารประกอบเชิงซ้อน 3C โปรทีเอส/สารยับยั้งที่เกี่ยวข้องกับโรคมือเท้าปาก

นางสาววารินทร์ เจษฎาวิสุทธิ์

วิทยานิพนธ์นี้เป็นส่วนหนึ่งของการศึกษาตามหลักสูตรปริญญาวิทยาศาสตรมหาบัณฑิต
สาขาวิชาเคมี ภาควิชาเคมี
คณะวิทยาศาสตร์ จุฬาลงกรณ์มหาวิทยาลัย
ปีการศึกษา 2559
ลิขสิทธิ์ของจุฬาลงกรณ์มหาวิทยาลัย

MOLECULAR MODELING ON 3C PROTEASE/INHIBITOR COMPLEXES INVOLVING HAND F
OOT MOUTH DISEASE

Miss Warin Jetsadawisut

A Thesis Submitted in Partial Fulfillment of the Requirements

for the Degree of Master of Science Program in Chemistry

Department of Chemistry

Faculty of Science

Chulalongkorn University

Academic Year 2016

Thesis Title	MOLECULAR MODELING ON 3C PROTEASE/INHIBITOR COMPLEXES INVOLVING HAND FOOT MOUTH DISEASE
By	Miss Warin Jetsadawisut
Field of Study	Chemistry
Thesis Advisor	Professor Supot Hannongbua, Ph.D.
Thesis Co-Advisor	Thanyada Rungrotmongkol, Ph.D.

Accepted by the Faculty of Science, Chulalongkorn University in Partial Fulfillment of the Requirements for the Master's Degree

　　　　　　　　　 Dean of the Faculty of Science

(Associate Professor Polkit Sangvanich, Ph.D.)

THESIS COMMITTEE

　　　　　　　　　 Chairman

(Associate Professor Vudhichai Parasuk, Ph.D.)

　　　　　　　　　 Thesis Advisor

(Professor Supot Hannongbua, Ph.D.)

　　　　　　　　　 Thesis Co-Advisor

(Thanyada Rungrotmongkol, Ph.D.)

　　　　　　　　　 Examiner

(Assistant Professor Somsak Pianwanit, Ph.D.)

　　　　　　　　　 External Examiner

(Pathumwadee Yotmanee, Ph.D.)

วารินทร์ เจษฎาวิสุทธิ์ : การสร้างแบบจำลองเชิงโมเลกุลของสารประกอบเชิงซ้อน 3C โปรทีเอส/สาร
ยับยั้งที่เกี่ยวข้องกับโรคมือเท้าปาก (MOLECULAR MODELING ON 3C PROTEASE/INHIBITOR
COMPLEXES INVOLVING HAND FOOT MOUTH DISEASE) อ.ที่ปรึกษาวิทยานิพนธ์หลัก: ศ. ดร. สุ
พจน์ หารหนองบัว, อ.ที่ปรึกษาวิทยานิพนธ์ร่วม: อ. ดร. ธัญญดา รุ่งโรจน์มงคล, 62 หน้า.

โรคมือเท้าปากนับเป็นโรคติดต่อชนิดหนึ่งที่พบบ่อยในเด็กเล็ก มักระบาดในช่วงฤดูฝน และบางครั้งมีการ
แพร่ระบาดอย่างรวดเร็ว โดยทั่วไปอาการของโรคจะไม่รุนแรงและหายป่วยได้เอง อย่างไรก็ตามการติดเชื้อเอนเทอโร
ไวรัส 71 (EV-A71) มักส่งผลให้มีอาการรุนแรงหรือภาวะแทรกซ้อนและทำให้เด็กเสียชีวิตได้ ในปีพ.ศ. 2554 พบการ
ระบาดของโรคมือเท้าในประเทศเวียดนามมากกว่า 1 แสนราย และมี 166 รายที่เสียชีวิตด้วยเชื้อ EV-A71 โรคมือ
เท้าปากพบได้ ในหลายประเทศ เช่น มาเลเซีย จีน สิงคโปร์ เวียดนาม บรูไน กัมพูชา และอังกฤษ เป็นต้น ปัจจุบันยัง
ไม่มีวัคซีนและยาต้านไวรัสที่ใช้รักษาอย่างจำเพาะ รูพินทริเวียร์ซึ่งเป็นสารยับยั้งที่มีประสิทธิภาพหลากหลายจึงเป็น
หนึ่งในตัวเลือกสำหรับใช้รักษาโรคมือเท้าปาก นอกจากนี้ SG85 เป็นสารยับยั้งที่ได้รับความสนใจเช่นกัน โดยมี
รายงานประสิทธิภาพการยึดจับระหว่างสารยับยั้งกับเอนไซม์ 3C โปรทีเอสของไวรัสที่ดีกว่ารูพินทริเวียร์เพื่อต้าน
คอกแซคกีไวรัสชนิด เอ16 (CV-A16) โดยสารยับยั้งทั้งสองมีประสิทธิภาพการยึดจับที่ดีใกล้เคียงกันเมื่อต้าน 3C โปร
ทีเอสของ EV-A71 ในการวิจัยข้อมูลเชิงโมเลกุลเพื่อศึกษาความชัดเจนในการยึดจับของสารยับยั้งทั้งสองชนิดข้างต้น
กับโปรทีเอส ผู้วิจัยมุ่งเน้นการศึกษาในสองส่วนหลัก คือการระบุกลไกการยับยั้งของสารยับยั้งที่มีประสิทธิภาพสูง
เช่น รูพินทริเวียร์ ในการต้านการทำงานของ 3C โปรทีเอส ใน CV-A16, EV-A71 และเอนเทอโรไวรัสชนิดดี 68 (EV-
D68) เพื่อเข้าใจการออกฤทธิ์ทางชีวภาพ และพัฒนาสารยับยั้งให้มีประสิทธิภาพยิ่งขึ้น โดยวิธีโมเลกุลลาร์ด็อกกิ้ง
และการจำลองพลวัตเชิงโมเลกุล (MD simulation) ซึ่งเป็นการใช้เครื่องมือทางคอมพิวเตอร์ ส่วนที่สองเน้นการ
ค้นหาสารประกอบจากฐานข้อมูล (ZINC, DrugBank, Scifinder และ ChemBL) เพื่อจำลองความสามารถในการ
ต้าน 3C โปรทีเอสของ CV-A16 และ EV-A71 โดยใช้เทคนิคการจำลองพลวัตเชิงโมเลกุลแบบสเตียร์ โดยอยู่บน
พื้นฐานที่ว่าหากแรงที่ใช้ดึงระหว่างโปรตีนกับลิแกนด์ออกจากกันมีค่ามาก จะส่งผลให้ประสิทธิภาพในการยึดจับที่ดี
จากการศึกษาพบว่าสารประกอบที่มีความคล้ายคลึงกับรูพินทริเวียร์ (analog of rupintrivir) โดยทำการดัดแปลง
หมู่ฟังก์ชันบริเวณ P2 ให้เป็นไฮดรอกซิลเมทิลในตำแหน่ง –meta และ –para ให้ค่าเฉลี่ยของแรงฉีกสูงกว่ารูพินทริ
เวียร์และ SG85 ซึ่งข้อมูลดังกล่าวจากทั้งสองส่วนของงานวิจัยสามารถนำไปใช้ประโยชน์สำหรับพัฒนาศักยภาพเป็น
ตัวยาต้านไวรัสโรคมือเท้าปากที่มีประสิทธิภาพต่อไป

ภาควิชา	เคมี	ลายมือชื่อนิสิต	....
สาขาวิชา	เคมี	ลายมือชื่อ อ.ที่ปรึกษาหลัก	....
ปีการศึกษา	2559	ลายมือชื่อ อ.ที่ปรึกษาร่วม	....

5772145223 : MAJOR CHEMISTRY

KEYWORDS: HAND, FOOT AND MOUTH DISEASE / MOLECULAR DYNAMICS SIMULATION / VIRTUAL SCREENING / STEERED MD SIMULATION / ENTEROVIRUS A71 / COXSACKIEVIRUS A16

WARIN JETSADAWISUT: MOLECULAR MODELING ON 3C PROTEASE/INHIBITOR COMPLEXES INVOLVING HAND FOOT MOUTH DISEASE. ADVISOR: PROF. SUPOT HANNONGBUA, Ph.D., CO-ADVISOR: THANYADA RUNGROTMONGKOL, Ph.D., 62 pp.

Hand, foot and mouth disease (HFMD) outbreaks frequently occur with children during the rainy season even becoming epidemic in some case. In general, HFMD patients have mild symptoms, that clear quickly. The enterovirus A71 (EV-A71) is a variant of the virus that causes severe pathogenic HFMD and may lead to death. In 2012, over 100000 HFMD cases were reported in Vietnam with 166 deaths due to EV-71 infection. HFMD occurrs in many countries e.g. Malaysia, China, Singapore, Vietnam, Brunei, Cambodia, and Great Britain. No vaccine or drug against HFMD is available. Rupintrivir, a broad-spectrum inhibitor, is a drug candidate for HFMD treatment, Another candidate is SG85, which is reported to have a better binding affinity than rupintrivir against CV-A16. Both inhibitors exhibit a comparable affinity against EV-A71 3C protease ($3C^{pro}$). In this work, the molecular information in term of the binding of the two inhibitors to the proteases will be elucidated. We aimed to investigate the inhibitory mechanisms of some potent compounds (e.g. rupintrivir) against the $3C^{pro}$ of the virus CV-A16, EV-A71 and EV-D68 in order to understand their biological activity and to develop procedures to improve their inhibitory potency. Molecular Docking and Molecular Dynamics simulation (MD simulation) are used as computational tools. The second part of this study is search for other potent HFMD inhibitors this was performed by screening several compound libraries (ZINC database, DrugBank and ChemBL) against the CV-A16 and EV-A71 3C proteases using steered molecular dynamic (SMD) simulations. Based on the hypothesis that a higher force is needed for pulling a more effective ligand from the protein target, the two analogs of rupintrivir containing the hydroxyl methyl at -meta and -para positions of the P2 side chain required an averaged rupture force higher than rupintrivir and SG85. The obtained information could be useful for the further development of anti-HFMD drugs.

Department:	Chemistry	Student's Signature	
Field of Study:	Chemistry	Advisor's Signature	
Academic Year:	2016	Co-Advisor's Signature	

ACKNOWLEDGEMENTS

CONTENTS

CONTENTS OF FIGURE

CONTENTS OF TABLE

CHAPTER I:

INTRODUCTION

1.1 Research Rationale

In 2012, Thailand was heavily affected from Hand, foot and mouth disease (HFMD). In particular, many children were infected by this disease and therefore, schools were closed during that time. Thailand was not the only country where this disease was found, but it was a global problem for several years. However, no vaccine or drug against HFMD is available up to now. Many cases of infected patients can recover within 1-2 weeks, but in some cases severe symptoms were observed with risk to die. This disease is caused by two main viruses, coxsackievirus A16 (CV-A16) and enterovirus A71 (EV-A71). 3C protease ($3C^{pro}$) is one of non-structural proteins, which plays a role to cleave some parts of polyprotein. The $3C^{pro}$ of the two main viruses have been crystalized together with rupintrivir, a potent inhibitor of this enzyme [1, 2], and these crystal structures can be found in the PDB database. C. Lacroix research group tested *in vitro* the activity of SG85 and rupintrivir with $3C^{pro}$ of EV-A71 [3], and they proposed both as drug candidates. Computational studies may play an essential role to support the experimental finding and to provide additional and extended information about inhibition mechanism. Both methods may lead to successful drugs against this specific disease. The following theoretical approaches will be applied:

I.   Key binding study: The binding between inhibitor and $3C^{pro}$ of viruses will be analyzed by molecular dynamics simulations.

In silico lead compounds: Steered molecular dynamics simulations play a role for better understanding of interaction of protein with the drugs and enable concerted screening of large databases in order to develop new drugs.

1.2 Hand foot and mouth disease (HFMD)

Hand foot and mouth disease (HFMD) is a common viral illness, which mainly affects infants and children younger than 5 years of age [4]. It can be transmitted through excretion of saliva and/or fecal matter [5]. This disease results in the inflammation of the skin, mouth, throat and legs. Moreover, the number of HFMD patients has continuously increased each year, especially in spring, summer and fall seasons [6, 7]. One of the main causes of HFMD is infection by viruses including CV-A16 and EV-A71. Most HFMD patients are commonly infected with CV-A16 [5]. In 2014, EV-A71 infections were reported about its infections in many countries including Taiwan [8], Singapore [9], Malaysia [10], Vietnam [11], Cambodia [12], Australia [13], China [14-18] and Thailand [19]. Disconcertingly, the EV-A71 variant can also cause neurological diseases (such as encephalitis), aseptic meningitis or polio [20, 21] and eventually may lead to death.

1.3 The main cause of disease

The CV-A16 and EV-A71 were identified as causes of epidemic HFMD disease in 2012. Recently, the Centers for Disease Control and Prevention (CDC) reported to occurrence of EV-D68 in 2014. They also cause neurological diseases like encephalitis, aseptic meningitis or polio disease [20, 21] that often eventually lead to fatality.
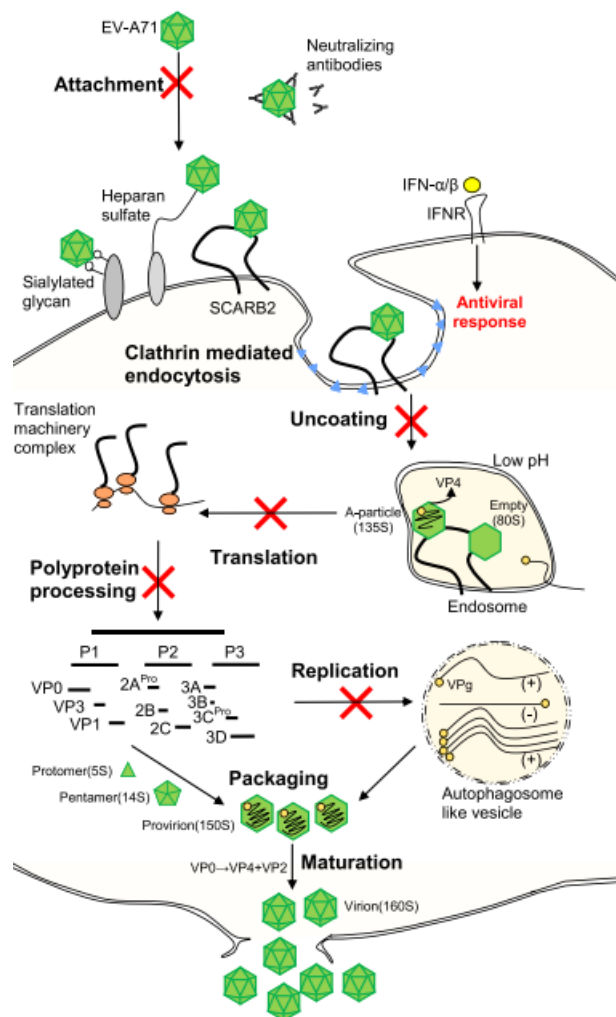
Figure 1 "Enterovirus life cycle" represents five stages of infection to host cell [22]

HFMD viruses are enterovirus genus [1] that are spherical and about 30 nm in diameter. The life cycle of enterovirus consists of five stages. Firstly, viral infection begins with initial attachment to receptor on the surface. Afterwards, they uncoated endosomes then absorb RNA to host cell before RNA translated, which the enterovirus genome is a positive stand approximately 7,000-8,500 nucleotides, to polyprotein that can be used as messenger RNA. The viral genomic RNA is transcribed into a complementary negative RNA that is used as a template to synthesize new stands of genomic positive RNA. Moreover, this chain protein has two parts: the structural and non-structural proteins. The structural part consists of 4 polypeptides, VP1, VP2, VP3 and VP4, that have been implicated as determinants encapsidation [23]. An important

point for this study is the non-structural protein consists of 7 junctions: 2A, 2B, 2C, 3A, 3B, 3C and 3D. 3A plays a role in the formation of the replication complexes (RCs). Viral protein synthesis and genomic RNA replication are catalyzed by RNA-dependent RNA polymerase, 3D, 2B, 2C, 3A and 3B [23, 24]. 2A protease (2A^{pro}) and 3C^{pro} are leader picornavirus-encoding proteases and special important to viral polyprotein process. The 2A^{pro} automatically cleaves a joint between VP1 and 2A^{pro}, while the other junctions are cleaved by 3C^{pro} [2, 25]. 3C^{pro} plays a key role in polyprotein processing of viral maturation, that favorably cleaves the peptide bond between glutamine (Q) and glycine (G) of viral protein through a reaction involving a catalytic triad of residues (H40, E71 and C147) [26]. Furthermore, the positive sense viral RNA are the packed to procapsid, that they mature to spread out virus particles in finally stage.

1.4 The crystal structure

The crystallography approach is studied to determine molecular structure. This study used 3D crystal structure, or 3D x-ray structure, in biological molecules from Protein Data Bank (PDB) which contains over 100,000 x-ray structures. There are thirteen human 3C^{pro} crystal structure, four structure of enterovirus type A and nine structure of enterovirus type D. However, only three crystals structure of the 3C^{pro} viral protein that interest as involved in the context; 3SJI, 3R0F, and 3ZVF. The first, 3SJI is crystal structure of human CV-A16 complex with rupintrivir (or AG7088) by Lu, G. et al. in 2011 [1]. The resolution was determined at 1.8 Å. Furthermore, 3R0F is 3C^{pro} of human enterovirus type A71 (EV-A71) complex with rupintrivir that mutant from Histidine to Glycine at residue 133. Wang, J. et al. [2] research group in 2011 determined the high resolution at 1.31 Å which was higher resolution than the previous studies. Although, the reported crystal structure has Histidine at residue position 133, the Glycine was changed to Histidine in this study. Most importantly, 3ZVF is 3C^{pro} of enterovirus type D68 (EV-D68) complexed with Michael receptor inhibitor SG85 that crystalized from Tan, J. et al. [27] in 2013. They are synthesized a series of peptidic α, β-unsaturated ethyl esters. SG85 is one inhibitor of 8 substrates in series that the highest potent activity. The PDB name is 3ZVF and resolution at 2.4 Å.

Table 1 Antiviral activities of CV-A16, EV-A71 and EV-D68.

Virus	inhibitor	PDB code	Activity (μM)	
			IC_{50}	EC_{50}
Coxsackievirus A16	Rupintrivir	3SJI[1]	2.06[1]	0.33[1]
	SG85	-	-	-
Enterovirus A71	Rupintrivir	3SJO[1], 3R0F[2]	1.65[1], 2.3[2]	0.78[1], ~1[2], 0.004[3], 0.018[28]
	SG85	-	-	0.18[27], 0.1[3]
Enterovirus D68	Rupintrivir	-	-	0.0046[28]
	SG85	3ZV8[27]	-	-

1.5 Treatment of HFMD
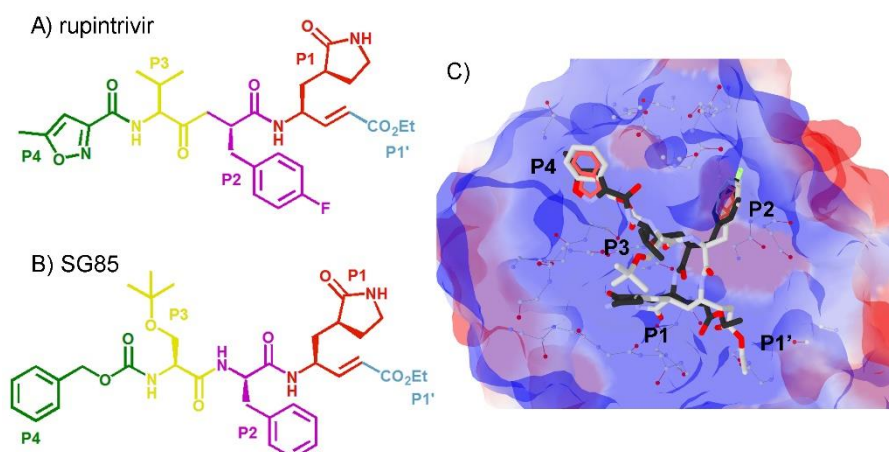
Figure 2 Chemical structures of A) rupintrivir and B) SG85 where the light blue, red, magenta, yellow, and green representing P1', P1, P2, P3, and P4 sites, respectively. C) Superimposed structures between rupintrivir (black) and SG85 (gray) in the active site of CV-A16 3C^{pro}.

Up to now, there has been very little data available about pharmacological studies regarding HFMD. For example, the ISI Web of Knowledge search revealed that

of the approximately 1,500 publications about HFMD, less than 2% of them related to the pharmacological aspects of HFMD. At this time, no drugs or vaccine are available to directly treat this disease. However, there are two candidate inhibitors currently under study. The candidate being studied first a peptide-based drug is rupintrivir or AG7088 (Figure 2A), a peptidomimetic with electrophilic ethyl propenoate Michael acceptor at C-terminal inhibitor, was preliminarily designed by Agouron Pharmaceuticals [29-32] to inhibit 3C^{pro} of the human rhinovirus (HRV). Recently, rupintrivir has been found to be a promising candidate for treating severe cases of EV-A71 infection *in vitro* studies with mice [33]. Moreover, rupintrivir has also shown a broad-spectrum antibiotic activity against viruses in the *Piconarviridae* family [29, 31, 34-36]. Nevertheless, this drug candidate is still *in vitro* study [26, 29, 30, 33, 37]. Also, it has low inhibition efficiency against 3C^{pro} of CV-A16. Additionally, EV-A71 exhibits the quite low inhibitory activity[1, 38, 39], the activity of rupintrivir against 3C^{pro} EV-A71 shows an IC$_{50}$ of 1.65 μM[1] and EC$_{50}$ of 0.78 μM[39]. The second drug candidate, SG85 (Figure 2B), is a member of the series of peptidic α, β-unsaturated ethyl esters, which is crystallized with 3C^{pro} of EV-D68. The x-ray structure of the SG85/EV-D68 complex is available in the PDB (PDB: 3ZVF) [27]. The biological activity of SG85 has been tested with several virus including EV-A71. SG85 displayed the highest inhibitory potency against EV-A71 3C^{pro} with EC$_{50}$ of 0.18 μM. Double mutations S127G and T143A of 3C^{pro} of Rhinovirus 14 had a low-level SG85 resistance but no cross-resistance with rupintrivir was reported [3]. However, no evidence and comparison between these two inhibitors in terms of intermolecular interactions and binding efficiency in molecular level at the active sites of CV-A16, EV-A71 and EV-D68 3C^{pro} enzymes are available.

1.6 Scope
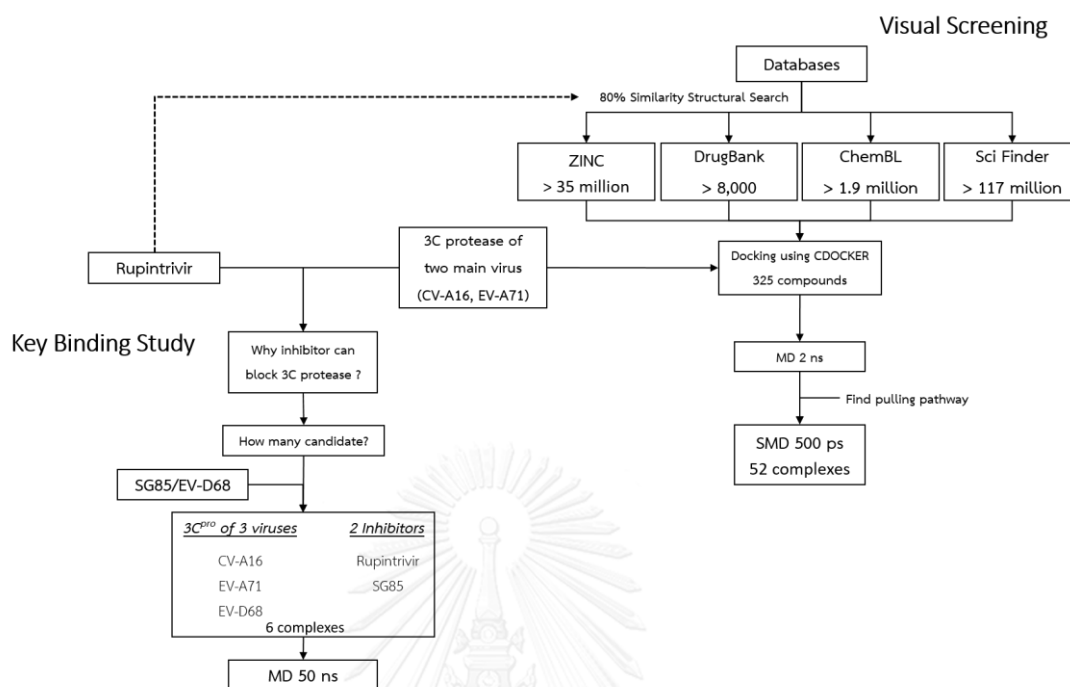
Figure 3 Schematic diagram of the approach of this study.

      This project is separated to two parts: Firstly, inhibitor and $3C^{pro}$ are indicated in key binding study part (left). In the second part of this study, computational techniques are used screen these compounds by predicting their anti-viral efficiencies (right).

CHAPTER II:

THEORETICAL

2.1 Molecular docking

Molecular docking research methods are used in structural molecular biology and computational drug design studies to investigate geometrical (*i.e.*, configurational) and energetic aspects of ligand-protein interactions. Normally, the molecular docking approach is used to study the accuracy of the enzyme structure and correct the predicted activity. In this work, a theoretical method was used to model the interactions an enzyme-inhibitor system. The method predicts the energy and three dimensional geometry of the enzyme-inhibitor complex. These predictions connect to the relative concentrations of the enzyme, inhibitor and complex that will exist in an equilibrium system. Free energy of binding will be considered by basic concept in Eq.1

$$[E]_{aq} + [I]_{aq} \overset{\Delta G_{bind}}{\leftrightarrow} [EI]_{aq} \qquad \text{Eq. 1}$$
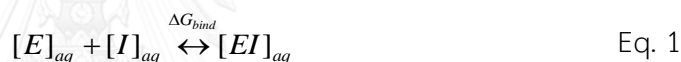
where $[EI]_{aq}$ is the complex between receptor and ligand, $[E]_{aq}$ is enzyme receptor and $[I]_{aq}$ is ligand.
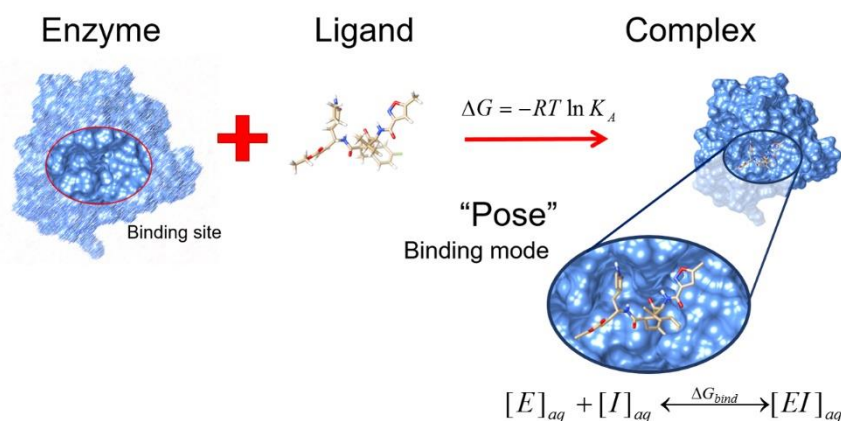
Figure 4 The basic concept is represented the molecular docking process to determine orientation of ligand that fit to the binding site of enzyme or receptor.

According to Figure 4, there are two components of the molecular docking method should be examined which are the scoring function and the search algorithm.
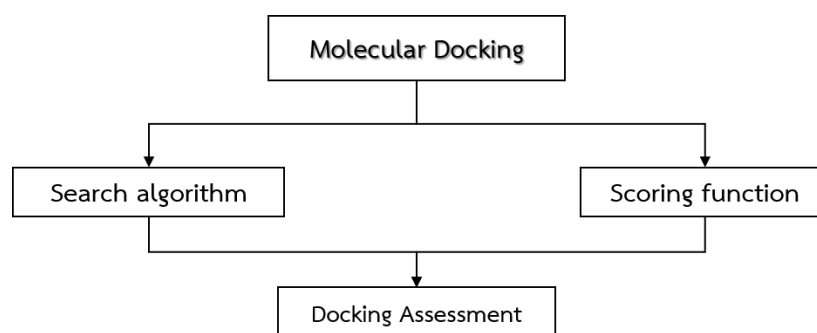
Figure 5 Scheme of the docking methodology

2.1.1 Scoring functions

The scoring function is used for estimating the binding affinities by observing the force field base and/or knowledge base, and comparing them to a library. The force field base is referred to functional form and parameter set that is used in molecular modeling field, especially the energy function or inter-atomic potential. Moreover, the knowledge base is a type of statistical observation that can be found from interaction of atoms or functional group. Besides, the random distribution is extracted from the basic knowledge base which can be compared with the experimental data.

2.1.2 Search algorithm

The overall search method is made of two types of searches: systematic and stochastic. The systematic search method involves finding space at predefined intervals and deterministic. The stochastic search method involves making random changes to the state variables to a user-defined termination criteria is met for find the local or global point. Many method tend to find near or local minimum energy point [40]. There are three main types involved in searching algorithm.

I) Molecular dynamics (MD) simulation [41]: This method is usually hold protein to rigid and allowed to freely explore their conformational space. Normally, MD simulation using a simulated annealing protocol to perform that support by a short MD energy minimization steps and rank overall energies scoring. In this study, the systems are used CDOCKER (CHARMm-based DOCKER) [42] program. This docking

studies observe from explicit all-atom, full force field, to represent protein is used. The accuracy is improved using grid-based approximation to explicit all-atom force field calculations. In final minimization step, protein is kept rigid while the ligands are treated as fully minimization step is used to refine the orientation poses. Molecular dynamics is applied the fully flexible ligand including bonds, angles and dihedrals, CHARMm is a force fields family. The one of important factor is grid, which represents interaction between protein-ligand. The grid origin was located at the center of active site that defines vdW or electrostatic probe. Ligand atoms were located between grid points. The grid's vdW interactions were generated in one of two ways, radii probe and distribution of atomic radii is a discrete probe. Additionally, each grid were generated the energies and forces with two option, the soft-core potentials in the heating-cooling stages and normal non-bond potentials in the final minimization step. The soft-core (E_{max}) was separated in three parts: van der waals interaction, electrostatic attraction and electrostatic repulsion, and can approximated by Eq. 2

$$E_{ij}(r_{ij}) = E_{max} - a \cdot r_{ij}^b \qquad if \ \left|E_{ij}^*\right| > \frac{\left|E_{max}\right|}{2} \qquad \text{Eq. 2}$$

where E_{ij}^* is the energy of the regular non-bond (vdW or electrostatic) potential. The coefficients a and b are parameters [43-45]. i and j represented to unbound state and bound state, respectively [45].

The binding free energy of CDOCKER program is predicted between ligand and receptor via basic concept in Figure 4. Using CHARMm based energies and implicit solvation methods. It is possible to estimate free energies and overall binding free energy. Note that, the receptor must be typed with the CHARMm force field. Therefore, the *in situ* minimization step is used to optimize the ligand in binding pocket. There are three steps of CDOCKER program calculate binding free energy. Firstly, ligand is minimized by *in situ*. Then, the entropy calculation is estimated from each conformation of ligand that is differs between initial ligand conformations and each

conformation change. Finally, the binding free energy is calculated in bound-unbound state using Eq. 3.

$$\Delta G_{binding} = E_{complex} - E_{protein} - E_{ligand}$$ Eq. 3

II) Shape-complementarity methods: These techniques used in commonly programs employ molecular docking programs such as DOCK [46], FRED [47] etc. These method describes the orientation which ligand molecules to bind with specific a proteins. The structure of interactions such as hydrogen bonding, hydrophobic contact, and van der Waals interactions are related to how well a particular ligand will bind with the protein target. Meanwhile, receptor structural present geometry using solvent-accessible surface area (SASA), the surface area of biomolecule that is accessible to a solvent. The descriptors can represent in form of structural templates quickly match potential compounds.

III) Genetic algorithms (GA): This method allow to exploring a large conformational space, which similar to an arrangement of the pair as a gene, in genetic biology, with particular energy. The each evolution of simulation is carried out by cross-over techniques, where random pair conformations are mated with a possibility for a random mutation in the offspring. The two programs well-known belong in class are GOLD [48] and AutoDock [49]. Although GA method is quite effective sampling the large conformational space, it is however limited in fixed protein and flexible ligand that used longer time in the process to calculate each generation. Recently, complementary-based approaches improve grid-based evaluation of energies, limit the conformational changes at only local areas or active site and improve tabling methods have significantly enhanced the performance of GA for suitable virtual screening.

2.2 Molecular mechanics (MM)

Molecular mechanics, force field method, is a model that is used to predict the energy of a molecule as a function of its conformation. Each of the atoms in a molecular mechanics calculation are treated like spherical points of mass and atoms that are bonded are held together by springs. As is described in Eq. 4, in a molecular mechanics calculation, the total energy is the sum of two terms: bonded and non-

bonded. The bonded term calculates the energies of bonded atoms. The non-bonded term calculates the energies of atoms that, although not being directly bonded, interact with each other by interactions such as Van der waal's forces. The potential energy in molecular scale can calculate by molecular mechanics due to molecular geometry. All-atomistic molecular mechanics method are specially to consider interaction of molecule including bond lengths, bond angle even in bond stretching. The each kinds of bond; single bond, double bond, triple bond or resonance, are effect to van der Waals attractions or electrostatic repulsions energy. The total potential energy can written in term of V via this equation:

$$V = V_{bonded} + V_{non-bonded}$$
$$V = (V_{bond} + V_{angle} + V_{dihedral} + V_{improper})_{bonded} + (V_{elec} + V_{vdW})_{non-bonded}$$

Eq. 4

This is alternative function of Potential energy functions (PEFs), is the knowledge-base or statistical. V is summation interaction between bonded term and non-bonded term concerning as the function of the positions, which consist of the Lennard-Jones (LJ) function; including van der waals attraction and repulsion of orbital overlap, and the Coulomb's law [50, 51].

2.2.1 Bonded energy

Bond stretching is one contribution in bonded term. The energy of a spring can approximately follow the Hooke's law like a spring in harmonic motion by

$$E_{bond} = \sum_{bonds} \frac{1}{2} k_b (r - r_0)^2$$

Eq. 5

where V_{bond} is the bond stretching function of each pair atom, k_b is the force constant of bond, r and r_0 are bond length between two atoms at actual state and equilibrium state, respectively. All bonds are summed by $\sum_{bonds}$ that were defined in system.

In the term of bending mode, represent angle between three atoms which consist of distortion between equilibrium angle position (θ_0) and present angle (θ). This energy term base on Hooke's law also

$$E_{angle} = \sum_{angle} \frac{1}{2} k_\theta (\theta - \theta_0)^2$$ Eq. 6

In addition, dihedral or torsion angle, the energy of torsional need to rotate the bonds and identify atom between four atoms. Normally, the torsion angle has important to single bonds that quite flexible than double bonds and triple bonds [52]. The torsional energy can defined by Eq. 7, where V_n is the rational barrier height, n is periodicity of rotation, τ is the torsion angle in conformation of molecule in that phase (ϕ)

$$V_{dihedral} = \sum_{dihedral} \frac{1}{2} V_n (1 + \cos[n\tau - \phi])$$ Eq. 7

Finally the energy in bonded term, improper, is defined from the small out-of-plane angle (α) and reference to four atoms but different from torsion angle. This term measure angle from three atom that is a plane to angle of bond from the top atom. The out-of-plane motional energy often necessary of planar group, example sp^2 hybridized, are represented by

$$V_{improper} = \sum_{improper} \frac{1}{2} V_n (1 + \cos[n\alpha - \psi])$$ Eq. 8

Therefore, k_ψ is the value of a spring constant, ψ_0 typically zero is used to restrain deformations among atom and three atoms bonded it. The ψ is defined to angle between the plane containing the first three atoms and the plane containing the last three
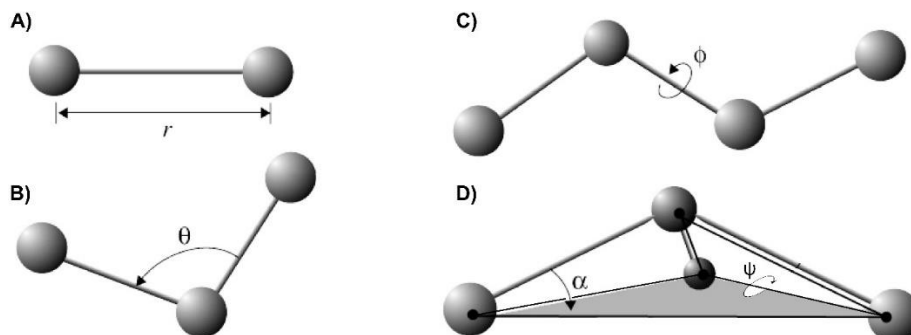
Figure 6 A) Bond stretching, B) bond angle, C) dihedral angel and D) improper torsion [53].

2.2.2 Non-bonded energy

The last energy comes from the non-bonded term that is separated into two parts: electrostatic energy, and van der Waals energy.

Electrostatic energy (V_{elec}) is one kind of interactions between two charge atoms and can represent with coulombic potential function as

$$V_{elec} = \frac{1}{4\pi\varepsilon_0} \sum_{ij} \frac{q_i q_j}{r_{ij}}$$

Eq. 9

where q_i and q_j are the charges on atoms i and j, respectively, r_{ij} is distance between them, the term $\frac{1}{4\pi\varepsilon_0}$ is the effective dielectric function for the medium. This function will get 1 when the system is in vacuum [52, 54-57]. The partial atomic charges possible to define charge distribution example dipole-dipole interaction which not represent more significant than simple point-charge model.

Van der Waals energy (V_{vdW}) is interaction between two atom from balance attractive and repulsive forces not only covalent or ionic bond [58] but also including force from Casimir effect arising from quantum interaction with zero-point energy [59]. The attractive force ($\frac{1}{r_{ij}^6}$) refer to dispersion force arises from fluctuations in charge distribution on electron cloud. The repulsive force ($\frac{1}{r_{ij}^{12}}$) happen when electron come to closely, electron-electron interaction will be strong. Normally van der Waals interaction using Lennard-Jones potential model, interaction depend on atom i and j express by equation below.

$$V_{vdW} = \sum_{ij} \frac{A_{ij}}{r_{ij}^{12}} - \frac{B_{ij}}{r_{ij}^6}$$

Eq. 10

where A_{ij} and B_{ij} are constant and r_{ij} refer to distance of pair-wise atom. The plot of Lennard-Jones potential model follow Figure 7.
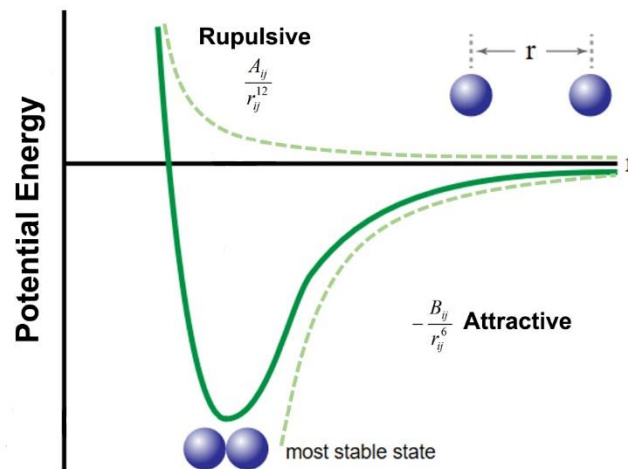
Figure 7 Van der Waals interaction based on Lennard-Jones potential

2.3 Molecular dynamics simulation (MD)

The simulation model can study in parallel with experimental in laboratory. It is important to remember that no one things can replace together, results from experimental cannot mention movement direction of molecules, cannot give specific energy to effect that situation etc., computer simulation come to prove any situation based on mathematic method and knowledge base from theoretical. MD simulation is one approach for study movement of molecules. Usually, the trajectories are determined using Newton's equations (Eq. 11) of motion to solve numerically for find energy in the last step. The potential energy is calculated from MM that mention in previous topic, in generally call "force field".

$$F_A = m_A a_A = m_A \frac{dv_A}{dt} = m_A \frac{d^2 r_A}{dt^2}$$ Eq. 11

The comparison between MM and MD are restrict of approaches. MM is a static different from MD is dynamics, example in bond length; MM will decrease the potential energy to reach. On the other hand, MD quite flexibility than MM that calculate energy till they stable in equilibrium state. In kinetic energy, MM calculate that ignorant but MD including potential and kinetic energy to conserve the system motion. However, the both method were still on oscillate based on Hooke's law. Figure 8 can explain the system of difference method.
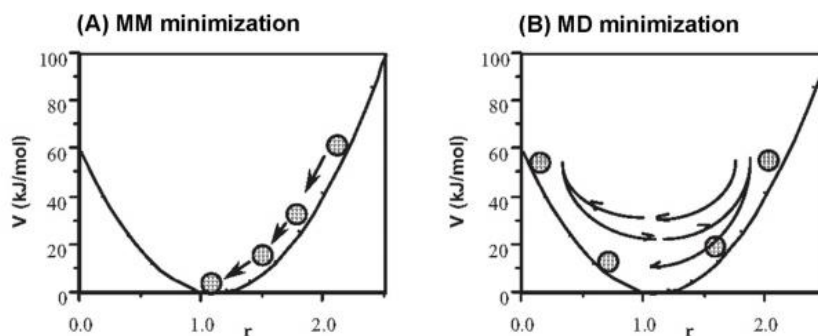
Figure 8 The comparison potential energy of bond length between MM and MD simulation [60].

2.3.1 Predictor algorithms

The molecular dynamics method using Newton's equation to solving motion of atom. The calculation happening from first step and re-calculated to find the new position. This process is repeated many thousands time in a typical simulation for satisfy the fundamental requirements about: accuracy atomic motion, stability of system energy/temperature, simplicity of program writing, calculation speed and used minimum of computer resources. The group of predictor algorithm is several forms for example separate to Verlet algorithm, Leab frog algorithm and velocity Verlet algorithm etc. which they are different slightly.

2.3.1.1 Verlet algorithm

The basic Verlet algorithm, it is used in this study, can solve from equation of motion via Eq. 12 then using Taylor expansion to find velocity in next step

$$v_i\left(t+\frac{\Delta t}{2}\right) = v_i(t) + \dot{v}(t)\frac{\Delta t}{2} + \frac{1}{2}\ddot{v}(t)\left(\frac{\Delta t}{2}\right)^2 + \ldots$$

$$v_i\left(t-\frac{\Delta t}{2}\right) = v_i(t) - \dot{v}(t)\frac{\Delta t}{2} + \frac{1}{2}\ddot{v}(t)\left(\frac{\Delta t}{2}\right)^2 - \ldots$$

Eq. 12

Then the difference of Taylor expansion above

$$v_i\left(t+\frac{\Delta t}{2}\right) - v_i\left(t-\frac{\Delta t}{2}\right) = \dot{v}(t)\Delta t$$

Eq. 13

After substitution by equation of motion (Eq. 11)

$$\frac{F_i(t)}{m_i} = \frac{1}{\Delta t}\left\{v_i\left(t+\frac{\Delta t}{2}\right)-v_i\left(t-\frac{\Delta t}{2}\right)\right\}$$

Eq. 14

The position (r) can do the same thing and give r from difference Taylor expansion for coordinate, which after take differential first order as

$$v_i\left(t+\frac{\Delta t}{2}\right) = \frac{1}{\Delta t}\left\{r_i(t+\Delta t)-r_i(t)\right\}$$

Eq. 15

Finally, this Equation substitute by equation of motion then velocities summarize give

$$v_i(t) = \frac{1}{2}\left\{v_i\left(t+\frac{\Delta t}{2}\right)-v_i\left(t-\frac{\Delta t}{2}\right)\right\}$$

Eq. 16

Moreover, Verlet algorithm can expansion to clarify using Figure 9 and Eq. 17 of basic Verlet method below.
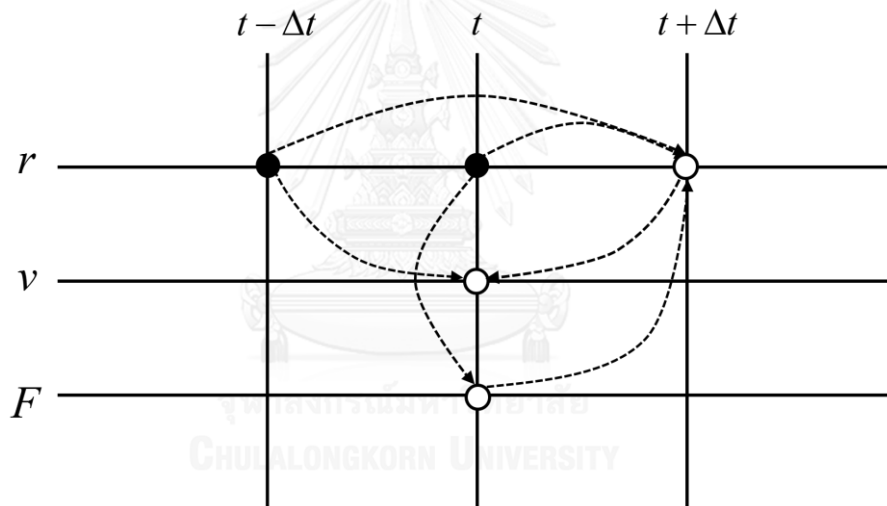
Figure 9 the explanation of basic Verlet algorithm starting from position at the present state then can find the previous time and calculate the future time [61].

$$r_i(t+\Delta t) = 2r_i(t) - r_i(t-\Delta t) + \frac{F_i(t)}{m_i}\Delta t^2$$

$$v_i(t) = \frac{1}{2\Delta t}\left\{r_i(t+\Delta t) - r_i(t-\Delta t)\right\}$$

Eq. 17

There are several advantages of basic Verlet algorithm. The integration does not requires the velocities that only position information is taken to calculation. Moreover, they use only a single force evaluation per integration cycle and this formulation based on forward-backward expansion, which naturally reversible in time.

In the other words, disadvantages of this method are error in velocity approximation about order of time step squared and need to know $r(n+1)$ to calculate $v(n)$. However, the numerical still imprecision in adding small and large numbers[61].

2.3.1.2 Leap Frog algorithm

Leap Frog algorithm is another choice of algorithm precision (Eq. 18). It can eliminates addition of small numbers to large ones and reduces the numerical error problem of Verlet algorithm. Moreover, this method is direct evaluation of velocities gives a useful handle for controlling the temperature in the simulation. In contrast, the velocities at time t are still approximation and use computational resource more than basic Verlet [61].

$$v_i\left(t+\frac{\Delta t}{2}\right) = v_i\left(t-\frac{\Delta t}{2}\right) + \frac{F_i(t)}{m_i}\Delta t$$

$$v_i(t) = \frac{1}{2}\left\{v_i\left(t+\frac{\Delta t}{2}\right) - v_i\left(t-\frac{\Delta t}{2}\right)\right\}$$

Eq. 18

2.3.1.3 Velocity Verlet algorithm

The last one for introduce is Velocity Verlet method. It is a second order integration scheme and self-starting; example when without reference into far past, the system at time Δt can calculated directly knowing only the system at time $t = 0$. In addition, it allow Δt to be chosen differently for each time. This can be very useful when the accelerations vary strongly overtimes and requires only one evaluation of the accelerations per time step [61]. Then, Veocities Verlet can explain by

$$v_i\left(t+\frac{\Delta t}{2}\right) = v_i(t) + \frac{F_i(t)}{m_i}\frac{\Delta t}{2}$$

$$v_i(t+\Delta t) = v_i\left(t+\frac{\Delta t}{2}\right) - \frac{F_i(t+\Delta t)}{m_i}\frac{\Delta t}{2}$$

Eq. 19

2.3.2 Periodic Boundary Condition

Molecular simulation system is investigated in condense phase or solution phase, for this study is solution phase. In real case, the system should be extremely solvated by solvent. However, the large number of molecules is difficult calculated which the approximation method is used to represent the environmental effect of the simulation system is periodic boundary conditions (PBC) method. In this approximation method, the infinitely soluble phase is generated by periodically repeated using a series of the identical finite system. Usually, the option method is used for three-dimensional extended in PBC approximation several shapes: cubic, truncates octahedral, triclinic etc.
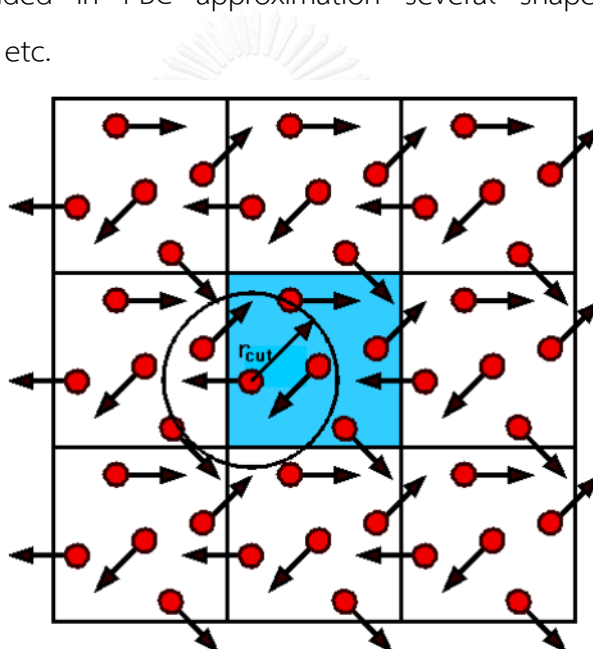
Figure 10 The PBC approximation in two-dimensions represented each system in square.

2.3.3 Particle mesh Ewald (PME)

The one of important methods, the particle mesh Ewald (PME), is approximate cutoff-based method. Ewald summation can be used for the full electrostatic energy calculation of unit cell (periodic box).

2.3.4 SHAKE algorithm

The SHAKE algorithm is often applied to molecular dynamics simulation for constraining some part of the system. It is first developed for satisfying a bond geometry constraint. In case of this study, it removed hydrogen motion that has frequency oscillation effects in the system.

2.4 Steered molecular dynamics simulation (SMD)

There are many reasons why steered molecular dynamics (SMD) is important and specific to ligand-receptor interactions in biochemical processes. This approach is used for dynamics study of bound/unbound states of the complex to investigate molecular interaction. SMD simulation is possible use to induce relatively large conformation changes in molecules on nanosecond time scales over MD simulation and not require expensive computational. Recently, the atomic force microscopy (AFM) is applied to study mechanical unfolding of biomolecule [62-64].
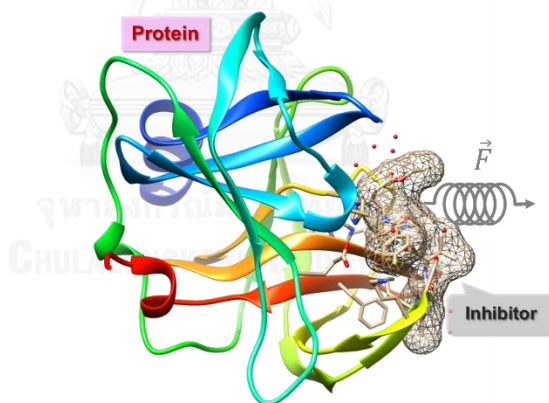
Figure 11 Steered molecular dynamics approach

The steered molecular dynamics (SMD) is an advance MD simulation techniques. This method was used to estimate binding energy of ligand to protein surface. In this study, main idea of method used to screen out lead compounds which based on the hypothesis that the larger is the force needed to unbind a ligand from receptor the higher its binding affinity. In addition, inter- and intra-molecular force are key to stability of biomolecules. While, ligand binding to receptor can estimate by

binding energy E_{bind} in equilibrium state and K is a equilibrium constant. According Eq. 20.

$$\Delta G_{bind} = -RT\ln(K)$$ Eq. 20

Under bound state between protein and ligand binding is applied the external force to pull ligand from binding pocket without fixing and atom of ligand. The force loaded with constant rate the total energy of protein-ligand complex as

$$V = V_{receptor} + V_{ligand} + V_{complex} + V_{force}$$
$$V_{force} = \frac{k}{2}(x - vt)^2$$ Eq. 21

where $V_{receptor}$, V_{ligand}, $V_{complex}$ are energy of receptor, ligand and complex interaction, respectively. Their forms depend on force fields used to describe the binding process. This approach is often compare to the Atomic-force microscopy (AFM) experiments that used spring constant of cantilever tip k around 10-1000 pN/nm. x is a displacement of atom position which the force is applied to atom, from the initial position. v is the pulling speed while kv is the force loading rate based on Hooke's law, $F = kx$ which is measured in experiments.

2.5 Binding Free Energies and Decomposition Free Energy

The molecular mechanics Poisson-Boltzmann surface area (MM-PBSA) approach was applied to estimate the binding free energy of the systems just to focus on the protein-ligand interaction only.

In AMBER program, the Binding Free Energy was calculated by the modules SANDER and PMEMD modules of AMBER14, following the Gibbs free energy equation (Eq. 22).

$$\Delta G = \Delta H - T\Delta S \approx \Delta E_{gas} + \Delta G_{solv} - T\Delta S$$ Eq. 22

The term ΔH can be approximated by $\Delta E_{gas} + \Delta G_{solv}$, where ΔE_{gas} is the summation energy of the complex in gas phase. ΔG_{solv} is the solvation energy calculated using the implicit solvent model. ΔS can be estimated using normal mode

approximation by a module available in AmberTools. The ΔH can be divided into two equations,

$$\Delta E_{gas} = \Delta E_{in} + \Delta E_{elec} + \Delta E_{vdW} \qquad \text{Eq. 23}$$

$$\Delta G_{solv} = \Delta G_{solv}^{polar} + \Delta G_{solv}^{nonpolar} \qquad \text{Eq. 24}$$

The internal energy ΔE_{in} represents the energy of bond, angle and dihedral angle contributions. Electrostatic energy ΔE_{elec} and van der Waals energies ΔE_{vdW} are taken with a cutoff of 12 Å. ΔG_{solv} comes from the terms of the solvation free energies in polar and nonpolar environments.

ΔG_{solv}^{polar} was estimated by Poisson-Boltzmann (PB) approximation [65-68] from eq. 25, and the non-polar solvation $\Delta G_{solv}^{nonpolar}$ [69, 70] is calculated using solvent accessible surface area (*SASA*) (Eq. 26). The surface tension constant (γ) is 0.0072 kcal/mol·Å^2.

$$\Delta G_{solv}^{polar} = -\frac{1}{2}(1 + \frac{e^{-Kf_{PB}}}{\varepsilon_\omega})\sum_{ij}\frac{q_i q_j}{f_{PB}} \qquad \text{Eq. 25}$$

$$\Delta G_{solv}^{nonpolar} = \gamma\, SASA \qquad \text{Eq. 26}$$

where the Debye-Hückel screening parameter (K) is defined as 80 for water phase and 0 for gas phase, the dielectric constant of solvent is ε_ω, and the last term f_{PB} is given in Eq. 27.

$$f_{PB} = \nabla \cdot \varepsilon(\vec{r})\nabla\phi(\vec{r})$$
$$= -4\pi\rho_0 - 4\pi\lambda\sum_i ez_i c_i \times \exp(\frac{-ez_i\phi(\vec{r})}{k_B T}) \qquad \text{Eq. 27}$$

where ϕ is the electrostatic potential and ε is the dielectric constant which they are variables functions of the position vector $\vec{r}$. ρ_0 is the solute charge density. λ is the ion-exclusion function, e is the unit charge, z_i and c_i are the valence and the number

density, respectively, of ion type i, k_B is the Boltzmann constant, and T is temperature. The variables ϕ and ε are functions of the position vector $\bar{r}$.

2.5.1 Per-residue Decomposition

The per-residue decomposition free energy ($\Delta G_{bind}^{residue}$) and its components, ΔG_{solv}^{polar}, $\Delta G_{solv}^{nonpolar}$, ΔE_{elec} and ΔE_{vdW} were calculated by MM-PBSA method. In the same way, the per-residue decomposition free energy contributed from backbone and side chain was estimated from the related atoms.

CHAPTER III:

METHODOLOGY

3.1 Preparation structure

3.1.1 Part I: Key binding study

The three crystal structures of the rupintrivir/CV-A16 3C^{pro}, rupintrivir/EV-A71 3C^{pro} and the SG85/EV-D68 3C^{pro} complexes were obtained from Protein Data Bank (PDB codes; 3SJI, 3R0F and 3ZVF, respectively) [1, 2, 27]. Note that the 3C^{pro} of CV-A16 shares a similar secondary structure of EV-D68 with 51.4% of identity and 73.5% of similarity and EV-A71 shares a similar secondary structure of EV-D68 with 52.5% of identity and 72.7% similarity. In order to prepare the complex structure between 3C^{pro} with SG85, both of their 3D structures were superimposed (3SJI-3ZVF and 3R0F-3ZVF). Both EV-D68 3C^{pro} and rupintrivir were sequentially removed. For the ionizable amino acids, their protonation states were then determined using PROPKA 3.1 [71]. Moreover, their environments were also examined as well, especially to histidine. The partial charges of the two ligands were prepared according to the previous studies [72-74]. The structures of these two complexes were fully optimization using HF/6-31G (d) implemented in the Gaussian09 program [75]. Subsequently, the electrostatic potential (ESP) charges were calculated with the same method. The restrained electrostatic potential (RESP) charges were carried out to convert from the ESP charges with antechamber module. The AMBER force field 03 (AMBER ff03) was applied for the protein [76]. Whilst, both AMBER ff03 and general AMBER force field (GAFF) [77, 78] were adopted for ligand parameters by parmchk program. The missing hydrogen atoms were added by the tLeap module implemented in AMBER 14.

3.1.2 Part II: Screening lead compounds

The crystal structures of the rupintrivir complexed with the 3C^{pro} of CV-A16 (Figure 12C) and EV-A71 (Figure 12D) were obtained from the Protein Data Bank (PDB entry codes 3SJI [1] and 3R0F [2]). These structures of the two viral proteases and

rupintrivir as the reference compound for structural similarity search from the four available databases, ZINC [79], DrugBank [80], ChemBL [81] and SciFinder[®] [82] were used for *in silico* screening of lead compounds in this study. Note that totally more than 50 million compounds were screened in this study. The molecules sharing similarity to rupintrivir at a 0.8 threshold and in addition the 13 rupintrivir analogs (Figure 12B) with a modification on the P2-site (Figure 12A).
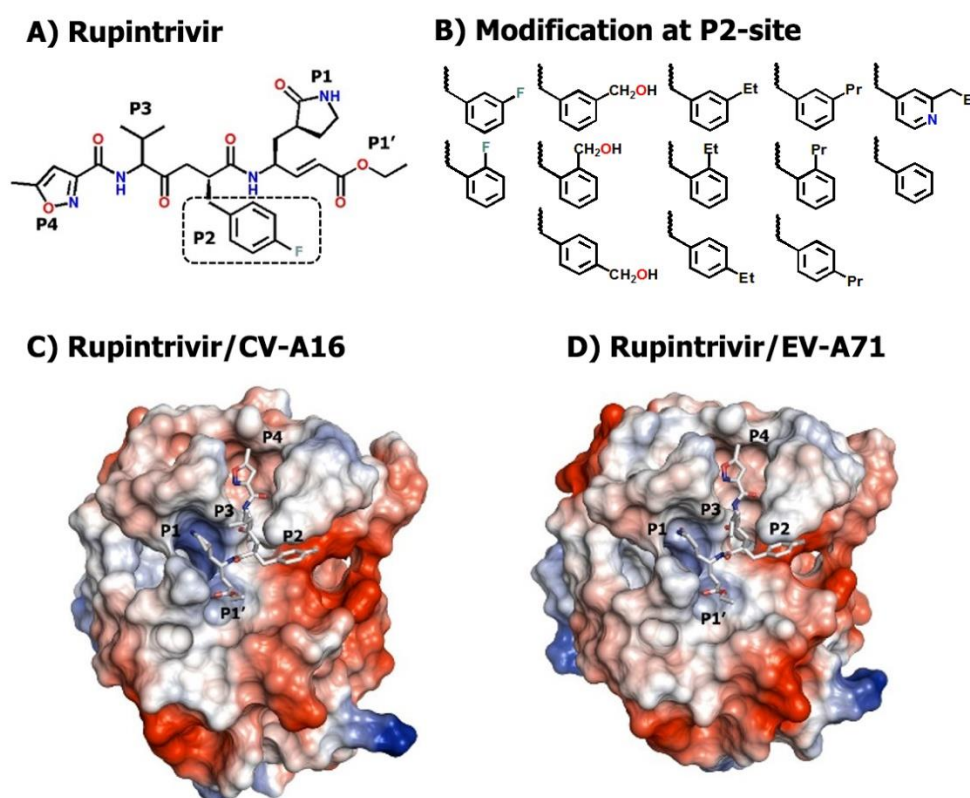
Figure 12 A 2D representation of A) rupintrivir (also known as AG7088). Note in the P2 group, which is modified in silico herein. B) The 13 modified functional groups vary - ortho, -meta, and -para positions at the P2-site of rupintrivir which from the left to the right is fluoro, hydroxy methyl, ethyl, propyl, propylpyridine, and benzyl, respectively. C) 3C[pro] of CV-A16 with rupintrivir bound at the pocket site (PDB code: 3SJI), rendered with a vacuum electrostatic surface in PyMOL software [83] showing negatively charged areas in red, and positively charged areas in blue. D) 3C[pro] of EV-A71 (PDB code: 3R0F) in complex with rupintrivir rendered with an electrostatic surface.

3.2 Molecular Docking

The CDOCKER [42] module in the Accelrys Discovery Studio 3.0[Accelrys Inc.] is used for individually docked ligand into the 3C[pro] active sites, after screen out using similarity search, to complexation. Based on the Momany-Rone method, the CHARMm force field was used for the molecular dynamics simulation and energy minimisation in docking procedure. The 100 random orientations of ligand were docked into the active site 11 Å sphere around. Once in the site, the whole system was annealed at 700K with 2000 steps and then cooled down in 5000 steps to the target temperature of 300K. The docked ligands were selected based on the interaction energy. Consequently, these compounds were fully optimized based on HF/6-31G(d) method using Gaussian09 program [75]. To prepare the Restrained Electrostatic Potential (RESP) charges of the ligand, Electrostatic Potential (ESP) charges of the ligand were calculated with the same method. The RESP charges of ligand produced by the antechamber package and general AMBER force field (GAFF) [84, 85] in AMBER14 program [86] were then converted to the GROMACS topology format using AnteChamber PYthon Parser interfacE (acepepy) [87] for MD and SMD simulations.

3.3. Molecular Dynamics simulation for target analysis

Each system was solvated by TIP3P water model [88] in a cubic box within 12 Å around protein surface, approximately 9100 water molecules. Additionally, each simulated system was then neutralized by a chloride ion. To remove the bad contacts and steric hindrances, the hydrogen atoms were firstly minimized with 10 steps of steepest descents (SD) and followed by conjugate gradient (CG) until it reached 1000 steps using SANDER module implement in AMBER14 [86]. Afterwards, the SD and CG minimizations with the same number of steps were applied to water molecules and the ions, whereas the protein and ligand were constrained with a force constant of 500 kcal/mol·Å^2. Finally, the whole system was fully minimized with the same procedure.

In this study, 50 ns of MD simulation of rupintrivir and SG85 complexes, and calculated simulation time step of 0.002 ps were performed with the standard procedure [89-91] under periodic boundary condition using SANDER implemented in

AMBER14. All covalent bonds implicated with hydrogen atoms were constrained using SHAKE algorithm [88]. The particle mesh Ewald method (PME) [92, 93] was used to treat the long-range electrostatic interaction, while the short-range cut-off 10 Å was applied for non-bonded interactions. Five separated stages in each complex were calculated. Firstly, to the system a force of 100.0 kcal/mol·Å^2 was applied to keep it motionless, the water molecules only can move, in NVE ensemble and temperature rises up from 0 to 310 K. The second stage, the residues around 5Å of inhibitor involving the inhibitor were kept constant by a force 50.0 kcal/mol·Å^2 following the last information from the first stage carrying on temperature of 310 K. In the third step, we applied a force to key residues (F25, H40, E71, L125, C147, H161 and F170) and the inhibitor of 25.0 kcal/mol·Å^2. Before the last stage to the inhibitor a force of 12.5 kcal/mol·Å^2 is applied. In each stage simulations over 500 ps were done, in totally 2 ns. The last stage for long simulation until 50 ns in NPT ensemble using pressure at 1 bar (0.987 atm) and compressibility of water at 44.6 ×10^{-6} bar^{-1} then unrestrained all systems and switch temperature regulation from Langevin dynamic to Berendsen method as well. In this final part trajectory are collected and the last 10 ns were taken for data analysis using the root-mean square displacement (RMSD) criterion. RMSD and hydrogen bond analysis were performed using CPPTRAJ modules [94] in Amber14.

3.4 Binding Free Energy and Decomposition Free Energy

The molecular mechanics Poisson-Boltzmann surface area (MM-PBSA) approach was applied to calculate the Binding Free Energy of the systems, using the last 10 ns (100 frames). Water molecules were omitted and replaced by an intrinsic water model, just to focus on the protein-ligand interaction only. The Binding Free Energy was calculated by the modules SANDER and PMEMD modules of AMBER14.

3.5 Steered Molecular Dynamics simulation for virtual screening

All system preparations and simulations under the periodic boundary condition were performed using the GROMACS-4.6.1 program package [95] using the AMBER ff03 [85, 96] and GAFF [84] force fields for protein and ligand, respectively. The protonation

states of the ionizable amino acids of the CV-A16 and EV-A71 proteases were assigned based on our previous work [97]. The complex was embedded in a box size of 7×7.5×10 nm with ~16,000 TIP3P water molecules [98]. After neutralization by Cl⁻ ions, the added waters and ions were energetically minimized using the steepest descent (SD) at 50000 step (water and ion, protein, and complex, respectively), while the other molecules were constrained, and conjugated gradient (CG) approaches at 20000 step to whole system. A time step of 2 fs and a cutoff distance at 1.0 nm for non-bonded interactions were used. The long-range electrostatic interactions were calculated using the particle mesh Ewald (PME) summation method [99]. Each system was heated to 310 K with the NVT ensemble using the Berendsen thermostat. Afterwards, the simulation with NPT ensemble was performed at 310 K and a pressure of 1 atm for 400 ps using the Parrinello-Rahman pressure coupling. The simulation was then equilibrated with the same condition for 1000 ps.

SMD is an advanced MD simulation that induces the ligand unbinding and conformational changes in biomolecules on time scales accessible to molecular dynamics simulation by applying an external force to pulling a ligand out of the active site [36]. To predict possible unbinding tunnels, the pulling path was identified using Caver 3.0 [20, 37, 38]. A tunnel connects a protein cavity with the bulk solvent. The size of a probe able to access internal cavity is limited by the radius of the tunnel gorge, the narrowest place in the tunnel [23]. After an equilibration phase, the bound ligand was pulled out from the binding pocket of the protease with constant velocity (v) of 0.005 nm/ps along the Z-direction using harmonic potential. A time step of 1 fs with van der Waals interaction cut off at 1.4 nm and the PME method was applied for the long-range electrostatic interactions. The C-alpha atoms of all amino acids were restrained, while the center of mass of ligand was pulled from 3C^{pro} along the Z-dimension by a spring constant (k) of 600 kJ/mol•nm^2 (~996 pN/nm). The total force can be measured via equation of $F = k(vt - x)$, where x is the displacement of the pulled atom from the starting position.

CHAPTER IV:
RESULTS AND DISCUSSIONS

4.1 Part I: Key binding study

4.1.1 Stability of the complexes

To obtain some information about the dynamic stabilities after equilibration of the four 3C^{pro}-inhibitor complexes, the root mean square displacement (RMSD) of each system relative to the initial energy minimized structures for all atoms of each snapshot versus simulation time was measured using the cpptraj module of AMBER14. The RMSD results are shown in Figure 13. The RMSD values of the 3C^{pro} of CV-A16, EV-A71 and EV-D68 in complex with rupintrivir were approximately found at 2.5, 2.2 and 2.8 Å, respectively. While the RMSD values of SG85/CV-A16 3C^{pro}, SG85/EV-A71 3C^{pro} and SG85/EV-D68 3C^{pro} complexes were ~2.4, ~2.2 and ~2.9 Å, respectively. Moreover, it is noticeable that there was conformational fluctuation around 0.25 Å from 3 ns until the end of simulation in all systems. Therefore, the last 10 ns of the trajectory was extracted for further analysis of the investigated systems.
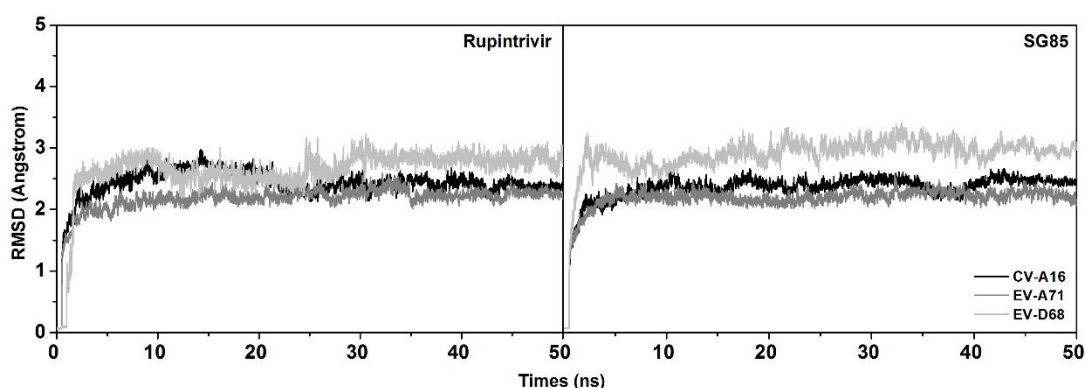
Figure 13 RMSD plots for the complex atoms of the CV-A16 (black), the EV-A71 (gray) and the EV-D68 (light gray) in complex with: left is rupintrivir and right is SG85.

4.1.2 Key Binding Residues of Inhibitor/3C^{pro} Complex

To scan the key residues important for inhibitor binding to 3C^{pro} of CV-A16, EV-A71 and EV-D68, the calculation of per-residue free energy decomposition ($\Delta G_{bind}^{residue}$) based on MM-PBSA method was applied from 40 to 50 ns. With an energy stabilization of less than 0.5 kcal/mol, the free energy from each residue showed that 3C^{pro} of CV-A16, EV-A71 and EV-D68 residues L125, L127, T142, A144, G163, N165 and F170 could be assumed to be stabilizing residues toward inhibitor binding, as shown in Figure 14. It should be noted that our finding is consistent with a previous study [26] in which the key binding residues of EV-A71/rupintrivir complex were L127, T142-C147, I162-N165 and F170. Moreover, the three additional binding residues including F25, H40 and S128 were found for the SG85 complexed with all protein complexes. This finding may reflect the stronger binding affinity of SG85 to 3C^{pro} of CV-A16 and EV-A71 than that of rupintrivir. However, it can be seen that the free energy decomposition value which is higher than 0.5 kcal/mol leads to a weaker binding affinity of the protein-inhibitor complex. This phenomenon is involved in repulsive electrostatic interaction. For example, the repulsive interactions between the residue I162 of three proteins and SG85 were investigated to have rather high unfavourable interactions around 2 kcal/mol (Figure 14). Meanwhile, the rupintrivir/CV-A16 complex displayed that this repulsive force was smaller than that of SG85 complexes (~1.5 kcal/mol).

For better understanding how the 3C^{pro} inhibitors with similar chemical structures interact with amino acid residues in the active site of 3C^{pro} of CV-A16, EV-A71 and EV-D68 the degrees of stabilization/de-stabilization from twenty three significant residues were separately considered with regard to contributions from their backbone atoms and from side chain atoms in Figure 15 (bar graph), together with the electrostatic ($\Delta E_{elec} + \Delta G_{solv}^{polar}$) and the van der Waals ($\Delta E_{vdW} + \Delta G_{solv}^{nonpolar}$) energies in Figure 15 (line graph) were analyzed. The results showed that most of the residues likely provided a degree of stabilization through their side chain, where the free energy from the residue atoms ($\Delta G_{bind}^{residue}$) was highly contributed from the side chain atoms in all complexes.

The main contribution of both compounds binding to the enzyme target came from the van der Waals interaction. Besides, it should be noted that although some amino acids behave slightly different for the considered complexes, the general shape of the binding sites of rupintrivir complexed with CV-A16, EV-A71 and EV-D68 as well as SG85 complexed with these three proteins are rather similar.
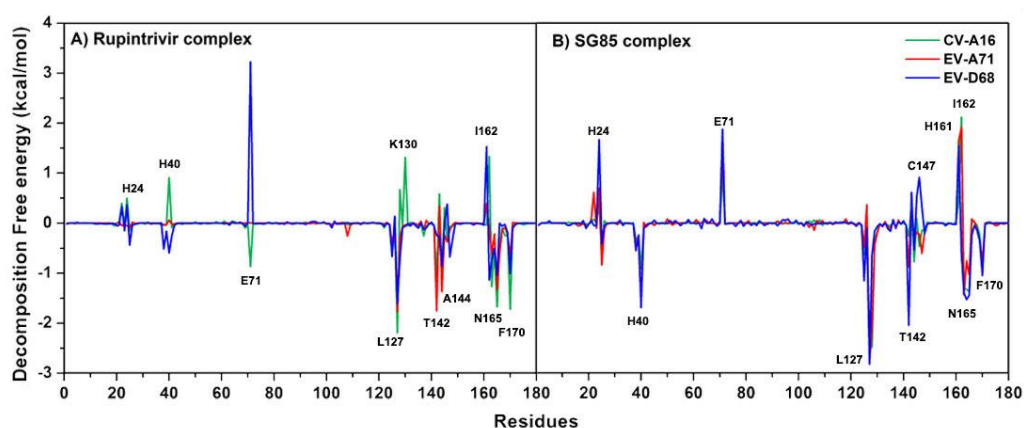
Figure 14 Per-residues decomposition free energy obtained from MM-PBSA calculation of the 3C^{pro} complexed with A) rupintrivir complex, B) SG85 complex. The green line is CV-A16, red line is EV-A71 and blue line is EV-D68.
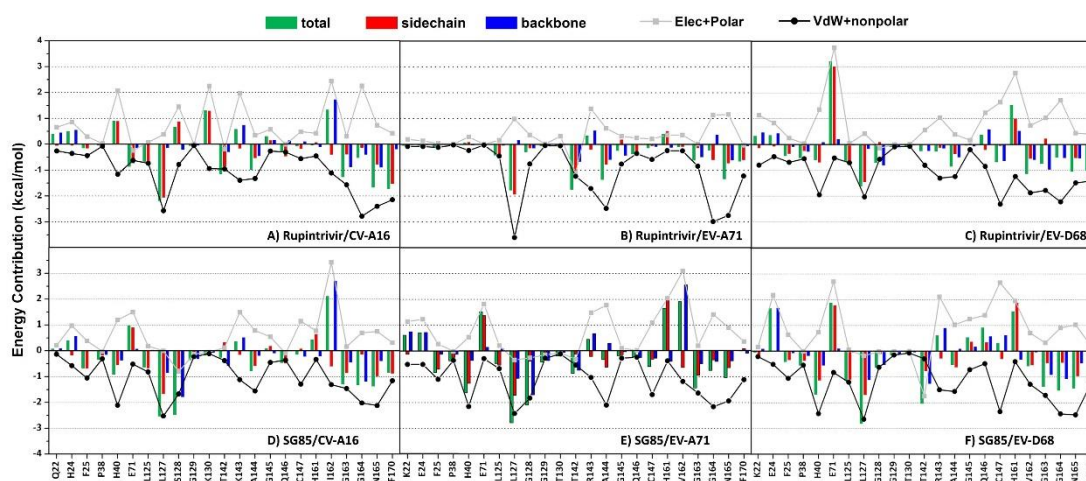
Figure 15 The data of MM-PBSA method analysis. The per-residue decomposition free energies are given as total energy (green bars), side chain (red bars) and backbone contributions (blue bars), while the electrostatic and vdW energy contributions are given in gray and black lines, respectively.

4.1.3 Intermolecular hydrogen bonds

To investigate the intermolecular hydrogen bonds between both inhibitors and 3C^{pro} of the two viruses from the last 10 ns MD trajectories. Hydrogen bonds were calculated in term of the percentage of hydrogen bond occupation. In accordance with the two geometric criteria are (i) a proton donor (D) and acceptor (A) distance ≤ 3.5 Å and (ii) a D–H···A bond angle ≥ 120°. The results and the schematics view of hydrogen bond interactions are given in Figure 16. For rupintrivir/CV-A16 complex, only one strong hydrogen bond was observed between the carbonyl oxygen on the P3-site of rupintrivir and the nitrogen backbone atom of G164. On the other hand, the complex of SG85/CV-A16 forms three strong hydrogen bonds at P1, P3 and P4 scaffolds with T142, G164 and S128, respectively. Guangwen Lu and co-workers [1] showed details of ten hydrogen bond interactions [100] of rupintrivir/CV-A16 complex from X-ray crystal stucture at different sites, including P1' to G145, P1 to T142/H161/I164, P2 to R39, P3 to G163/G164/S128 and P4 to G164/N165. The crystal structure of rupintrivir/EV-A71 of Jing Wang and co-worker [2] presented several possible hydrogen bonds, *i.e.,* P1' to G145, P1 to T142/H161/I162/G163, P2 to R39, P3 to G163/G164 and P4 to S128. In the complexes with EV-A71, rupintrivir forms two strong hydrogen bonds at P3-site with G164 and P4-site with S128, while SG85 could additionally interact at P1-site with T142. In addition, EV-D68 was keep interaction with SG85 than rupintrivir at P1-site with T142, P3 with G164 and P4 with L127. Furthermore, this study is give informations similar to research from Lacroix, Céline et al. [3] that suggested SG85 to promises drug candidate for treat virus in enterovirus genus type A.

A) Hydrogen bond of each complex

B) Rupintrivir/CV-A16

C) SG85/CV-A16

D) Rupintrivir/EV-A71

F) Rupintrivir/EV-D68

F) SG85/EV-A71

G) SG85/EV-D68
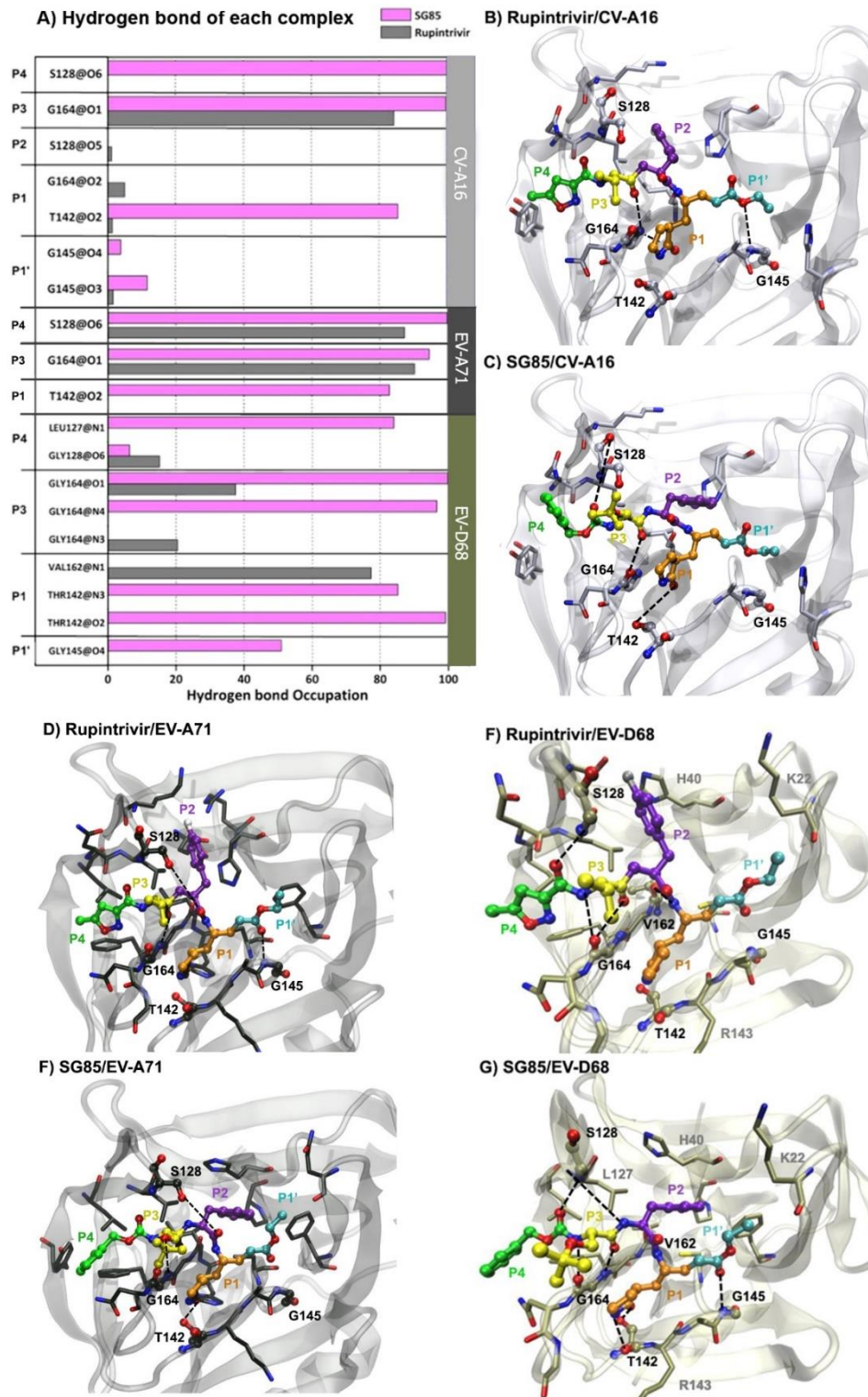
Figure 16 Hydrogen bonding interaction between 3C^{pro} and potent compounds from the last 10 ns simulation A) together with the structures of the binding pockets obtained from the last snapshot (B-G)

4.1.4 Binding free energy of inhibitor-protein complexes

To estimate the binding free energies of complexes in aqueous solution, the MM-PBSA method was performed. On the basis of this approach, it combines the molecular mechanical energies with the calculation of the free energy of solvation. The Poisson–Boltzmann (PB) method was applied to calculate the electrostatic contributions to the solvation free energy with a numerical solver, whilst the nonpolar component is evaluated from the solvent accessible surface area (SASA). In general, the binding free energy of the complex can be calculated by the free energy difference between the complex, protein and inhibitor. The energetic components consist of the gas phase energy (ΔE_{MM}) obtained from the summation of electrostatic (ΔE_{elec}) and van der Waals energies ΔE_{vdW}, solvation free energy (ΔG_{solv}) and entropy contribution ($T\Delta S$). The predicted binding free energies and their corresponding energy contributions of all systems, as well as the experimental binding free energy (ΔG_{exp}) converted from IC_{50} values of rupintrivir in complex with both viral enzymes are given in Table 2.

Table 2 The results from MM-PBSA approach giving the energy components and average binding free energies for the complexes of both inhibitors with the two targeted enzymes in comparison with experimental values.

MM-PBSA	CV-A16		EV-A71		EV-D68	
	Rupintrivir	SG85	Rupintrivir	SG85	Rupintrivir	SG85
ΔE_{elec}	-13.5 ± 4.1	-37.6 ± 4.8	-6.8 ±2.9	-36.7 ±4.3	-20.6 ±4.7	-37.7 ±4.8
ΔE_{vdW}	-54.9 ± 4.3	-54.1 ± 4.7	-43.5 ±2.6	-57.2 ±3.6	-57.8 ±3.4	-60.9 ±3.0
ΔE_{MM}	-68.4 ± 7.0	-91.7 ± 4.8	-50.3 ±3.9	-93.9 ±4.3	-78.4 ±4.0	-98.6 ±3.9
ΔG_{solv}^{polar}	39.6 ±5.6	59.3 ±4.0	24.4 ±3.2	62.8 ±3.5	46.9 ±4.5	65.2 ±4.2
$\Delta G_{solv}^{nonpolar}$	-5.0 ±0.3	-4.9 ±0.3	-3.8 ±0.2	-5.0 ±0.2	-4.9 ±0.2	-4.7 ±0.2
ΔG_{solv}	34.6 ±5.4	54.4 ±3.8	20.6 ±3.0	57.8 ±3.4	42.0 ±2.4	60.5 ±2.2
$\Delta E_{elec} + \Delta G_{solv}^{polar}$	26.1 ±4.8	21.7 ±4.4	17.6 ±3.0	26.1 ±3.9	26.3 ±4.6	27.5 ±4.5
$\Delta E_{vdW} + \Delta G_{solv}^{nonpolar}$	-59.9 ±2.3	-59.0 ±2.5	-47.3 ±1.4	-62.2 ±1.9	-62.7 ±1.8	-65.6 ±1.6
ΔH	-33.8 ±4.0	-37.3 ±4.9	-29.6 ±2.3	-36.1 ±4.8	-36.4 ±4.4	-38.2 ±4.7
$-T\Delta S$	-26.8 ±2.0	-26.1 ±3.0	-26.5 ±4.4	-26.4 ±2.8	-24.9 ±3.7	-29.5 ±5.8
ΔG_{bind_cal}	-6.9 ± 4.5	-11.2 ± 5.8	-7.8 ±2.3	-7.8 ±4.8	-11.5 ±5.8	-8.7 ±7.4
ΔG_{bind_ref}	-7.8 *	NA	-7.9 *	NA	-6.8 ±2.9	-36.7 ±4.3
$k_{obs}/[I]$ $(M^{-1}s^{-1})$	NA	NA	NA	NA	NA	202,200 ±8,103 ***
IC_{50} (μM)	2.06 ±0.14 *	NA	1.65 ±0.10 * / 2.3 ±0.5 **	NA	0.0046 ***	NA

* Lu G. et. al., *Journal of virology*, **2011**, 85(19), 10319-31   ***Donald F. Smee et.al., *Antiviral research*, **2016**, 131, 61-65
** Wang J. et. al, *Journal of virology*, **2011**, 85(19), 10021-10030

Taking into account molecular mechanics calculation in gas phase (ΔE_{MM}), the attractive electrostatic contributions (ΔE_{elec}) between SG85 and three proteins were similar in these three complexes (~ -37 kcal/mol), while the rupintrivir/EV-A71 system showed stronger ΔE_{elec} by approximate 2-fold than that of rupintrivir/CV-A16 except rupintrivir/EV-D68 around -20 kcal/mol. In addition, van der Waals interaction (ΔE_{vdW}) was found to be of similar values (-54 to -60 kcal/mol) in five complexes (rupintrivir/CV-A16, rupintrivir/EV-D68, SG85/CV-A16, SG85/EV-A71 and SG85/EV-D68). This is true except for the complexation of rupintrivir/EV-A71, which displays the highest value of vdW energy contribution. However, the vdW interaction could be considered as the key driving force in forming the complex of these systems. It can also be seen that the binding affinity of SG85/CV-A16 was higher than that of rupintrivir/CV-A16 by ca. 4 kcal/mol, while both inhibitors had the same ability to bind to 3C^{pro} of EV-A71 (~8 kcal/mol). Moreover, it is able to notice that the predicted total binding free energies (ΔG_{bind_cal}) of rupintrivir complexed with both viral proteins are in good agreement with the experimental data.

4.2 Part II: Virtual screening

4.2.1 Screening by similarity search and molecular docking

The 3C^{pro} enzymes of CV-A16 and EV-71 with rupintrivir bound (PDB ID: 3SJI [1] and 3R0F [101]) used in this study have a sequence identity of 90% folding into a similar secondary structure (RMSD of 0.6 Å), and show likely related binding residues around the rupintrivir and SG85 (residue identity 91% and similarity 96% [97]). Therefore, it can be expected that a molecule which effectively inhibits one protease might correspondingly exhibit antiviral activity against another target. Based on the 0.8 threshold structure similarity to rupintrivir, the 190 ZINC, 28 DrugBank, 16 ChemBL and 89 SciFinder® compounds were screened (Figure 17). These 323 compounds and in addition the 13 rupintrivir analogs were then docked into the 3C^{pro} active site of both proteases. Note that the P2-site of rupintrivir was modified in order to better interact with H40, E71, S128, and K140 of 3C^{pro}. The CDOCKER interaction energy between ligand and 3C^{pro} choosed the best 50 complexes. Finally, the top 52 molecules (Figure 18), including rupintrivir and SG85, were more precisely simulated using SMD from the active site of 3C^{pro}.
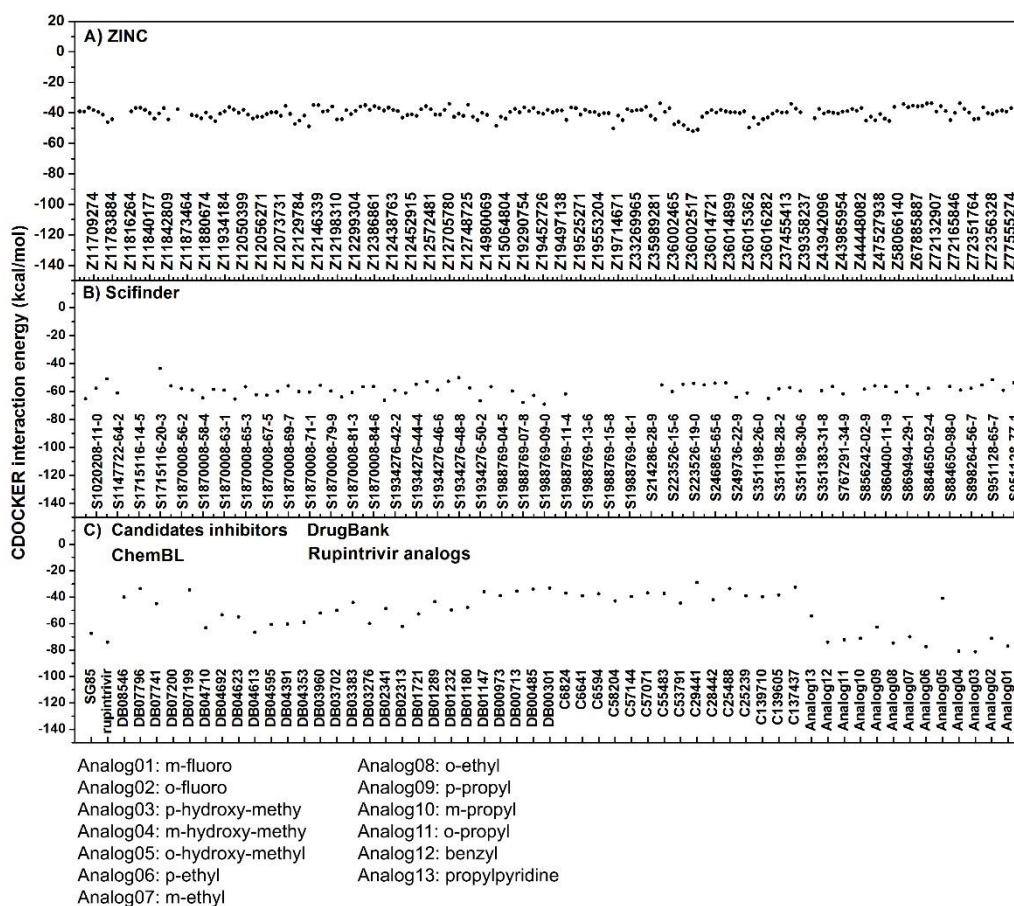
Figure 17 The docking score of complex of EV-A7 3C^pro with compounds obtained from A) ZINC, B) Scifinder, and C) Candidates, DrugBank, ChemBL, and rupintrivir analogs.

Analog01: m-fluoro
Analog02: o-fluoro
Analog03: p-hydroxy-methy
Analog04: m-hydroxy-methy
Analog05: o-hydroxy-methyl
Analog06: p-ethyl
Analog07: m-ethyl
Analog08: o-ethyl
Analog09: p-propyl
Analog10: m-propyl
Analog11: o-propyl
Analog12: benzyl
Analog13: propylpyridine
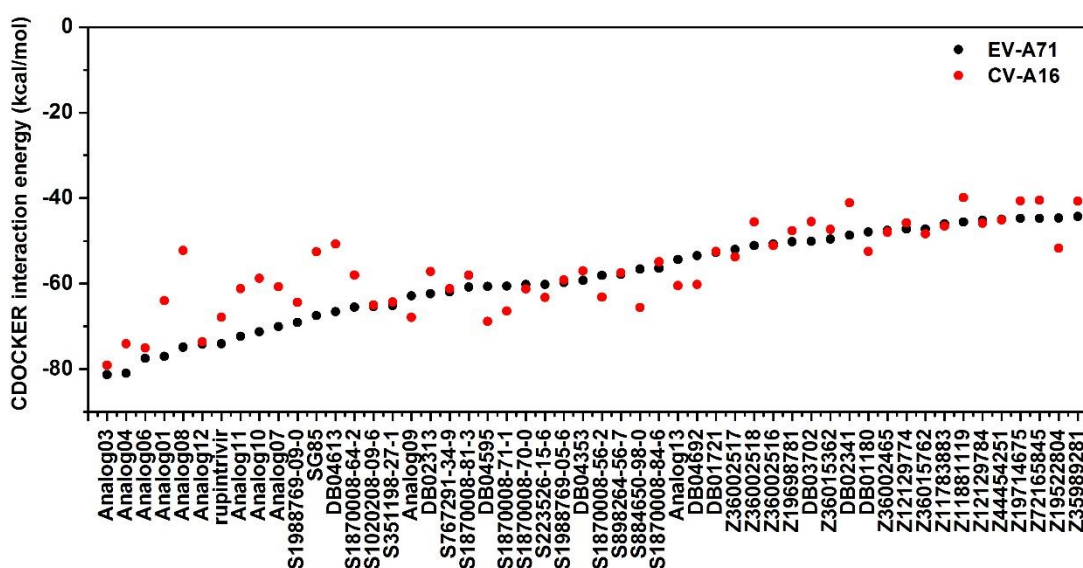
Figure 18 The top 52 compounds obtained by SMD method.

4.2.2 Choice of pulling pathway

A) Coxsackievirus A16

Pathway	Depth (nm)	Radius (nm)
1	8.95	1.51
2	27.93	1.17
3	27.32	1.18
4	38.26	1.13
5	43.71	1.05

B) Enterovirus A71

Pathway	Depth (nm)	Radius (nm)
1	9.10	1.56
2	20.84	1.02
3	27.59	1.03
4	32.00	1.24
5	33.52	1.17
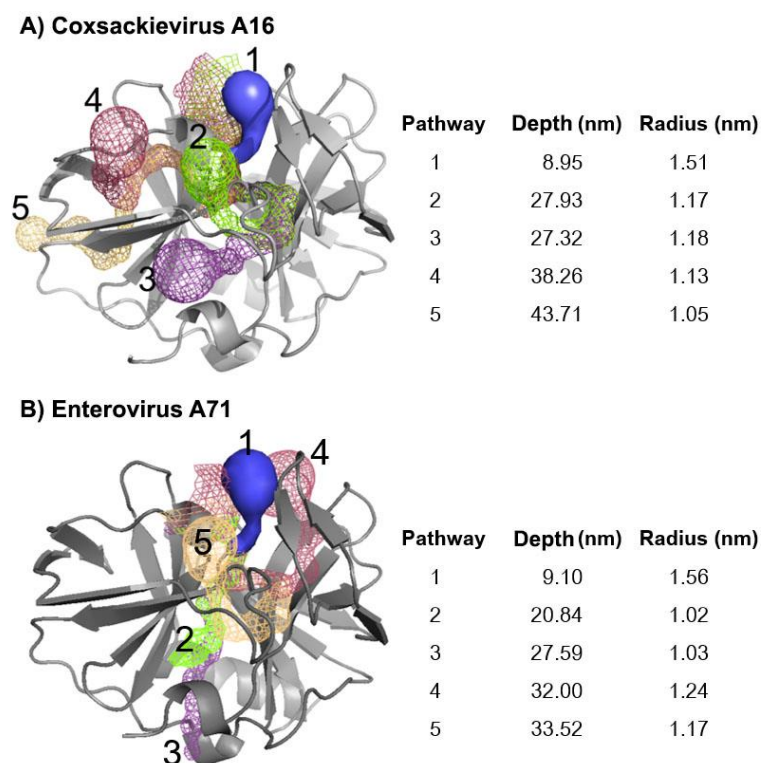
Figure 19 The 5 possible pulling pathways with average depth and radius for ligand unbinding from the 3C[pro] binding site of CV-A16 and EV-A71 calculated by CAVER plugin [102-106].

The choice of path is calculated to find tunnels and channels that the pulling path is sensitively reacted with the rupture force. SMD pulls the ligand out from the active site with a constant vector. To determine which is the most biologically relevant pathway to satisfy the pulling vector (the pulling pathway), that several routes to the active site must be quantitatively assessed. The shape of the protein tunnel can be approximated as a pipeline with a varying width of the cross section. The pulling pathway is chosen based on the hypothesis that the easiest pathway for the ligand to get away from the active site would have the largest width and the shortest depth length [102, 103, 106]. From the possibility of pulling pathways, the 3C[pro] of EV-A71 and CV-A16 are found five tunnels. Here, the chosen pathway 1 (Figure 19) conforms the best to this concept since it is both the shallowest, and has the widest pathway available. Around 4 Å of the tunnel to the active site are seven residues including E71, R39, P38, H40, I162, L127 and S128. In addition, it should be noted that the important

catalytic residues consists of H40, E71 and C147 which play a key role to proteolysis when the substrate is bound in near region; the pathway does not interfere with the proteolysis. Note that the first pathway of CAVER plugin similar to tunnels were calculated by MOLE 2.0 program version 2.5.13.11.08 and visualized using PyMOL 0.97rc that include in PDB sum of EMBL-EBI 2016 [107].

4.2.3 Ranking of binding affinity of ligands by SMD results

The validation data is reported to compare SMD approach with Jinzhi Tan *et al.* experimental values of EC_{50} values of EV-A71 3C[pro] bound with the SG-series of compounds [27]. They displayed the strongest interaction with SG85 (1.0±0.2 µM) and a lesser extent to SG98 (2.5±0.5 µM), and SG75 (7.0±1.1 µM). In the current study, as a trend we do indeed corroborate these rankings *in silico* demonstrating the accuracy of the models. SG85 is the best predicted high potent compound that is pulled at around 470 kJ/mol·nm, SG98 is less effective (280 kJ/mol·nm) and SG75 has weaker binding still (190 kJ/mol·nm) that are represent in Figure 20. The SMD results are in the same trend with experimental data that reported. Therefore, it would be confirmed that the SMD approach is a promising tool to estimate the inhibition efficacy of an inhibitor against the 3C[pro]. The SMD approach is in consistent with many researches of Mai Suan Li and co-worker to report this method is a promising tool for drug design [62, 74, 108-110].
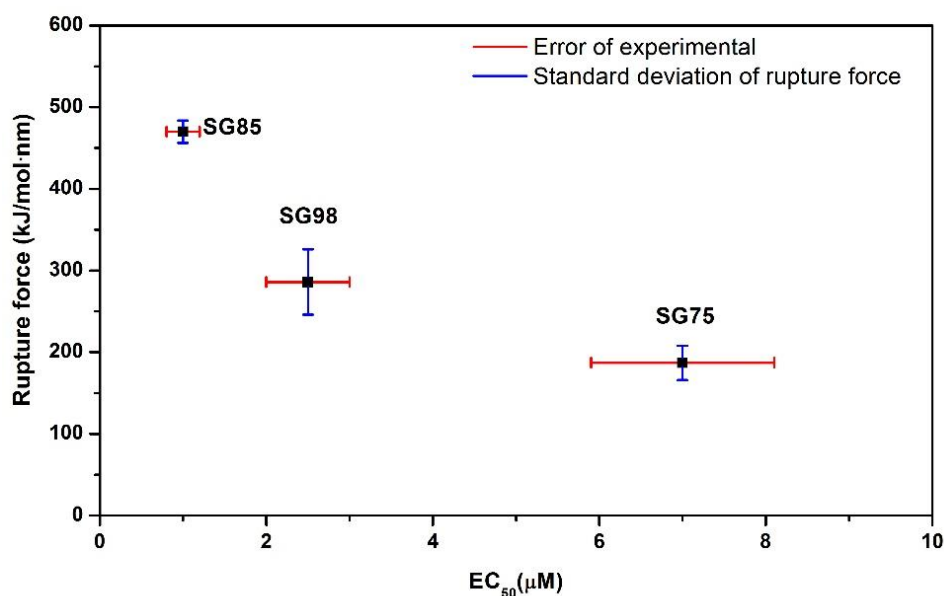
Figure 20 The comparison between the rupture force and the half-maximal effective concentration (EC_{50}). Blue line represented the standard deviation of rupture force in three time. Red line represented the error reported from experimental.

SMD simulations were performed for the found complexes that were compared the rupture force with rupintrivir and SG85 systems from 50 complexes in EV-A71 and CV-A16. The rupture forces of the 52 compounds in each variant of $3C^{pro}$ were ranked (Figure 4). Rupintrivir was required an average rupture force $\left(F_{avg}\right)$ value of ~510 kJ/mol·nm for CV-A16 and ~430 kJ/mol·nm for EV-A71. While, the rupture force of SG85/EV-A71 and SG85/CV-A16 about ~470 kJ/mol·nm and ~540 kJ/mol·nm, respectively. The discrepancy of SG85 better than rupintrivir in EV-A71 $3C^{pro}$ that expressed in terms of rupture force. Although, the previous study reported in term of binding free energy that affinities of both inhibitors are rather comparable [97]. This observation is in contrast with bioactivity assay that published by Céline Lacroix [3]. Whereas, This rupture force of rupintrivir and SG85 of CV-A16 data are good agreement that found by previous study [97] since 2016. Meanwhile, analogue of rupintrivir are modified by hydroxy methyl at -meta position (Analog04) that used force ~630 kJ/mol·nm, the analogue of rupintrivir modification by hydroxy methyl at -para position (Analog03) as ~580 kJ/mol·nm require higher pulling forces than rupintrivir and SG85 complexed with CV-A16. In the EV-A71 system, even more compounds were found to

require a higher pulling force than rupintrivir and SG85: Analog07, Analog12, Analog01, Analog09, Analog04, Analog13, ZINC19522804, DB04595, Analog03 (Figure 21). Whereas, 1020208-09-6 from Scifinder data better than rupintrivir but not higher force than SG85 in CV-A16 system. In case of EV-A71, Analog06 and 223526-15-6 are similar situation. On the three time running simulation were got standard deviation exceed ±50 kJ/mol•nm. We found that analog04, analog03 can more potently bind to both $3C^{pro}$ variants than rupintrivir and SG85. This data of SG85 is promise drug candidate good agreement that Lacroix Céline [3] reported by biological activity since 2015.
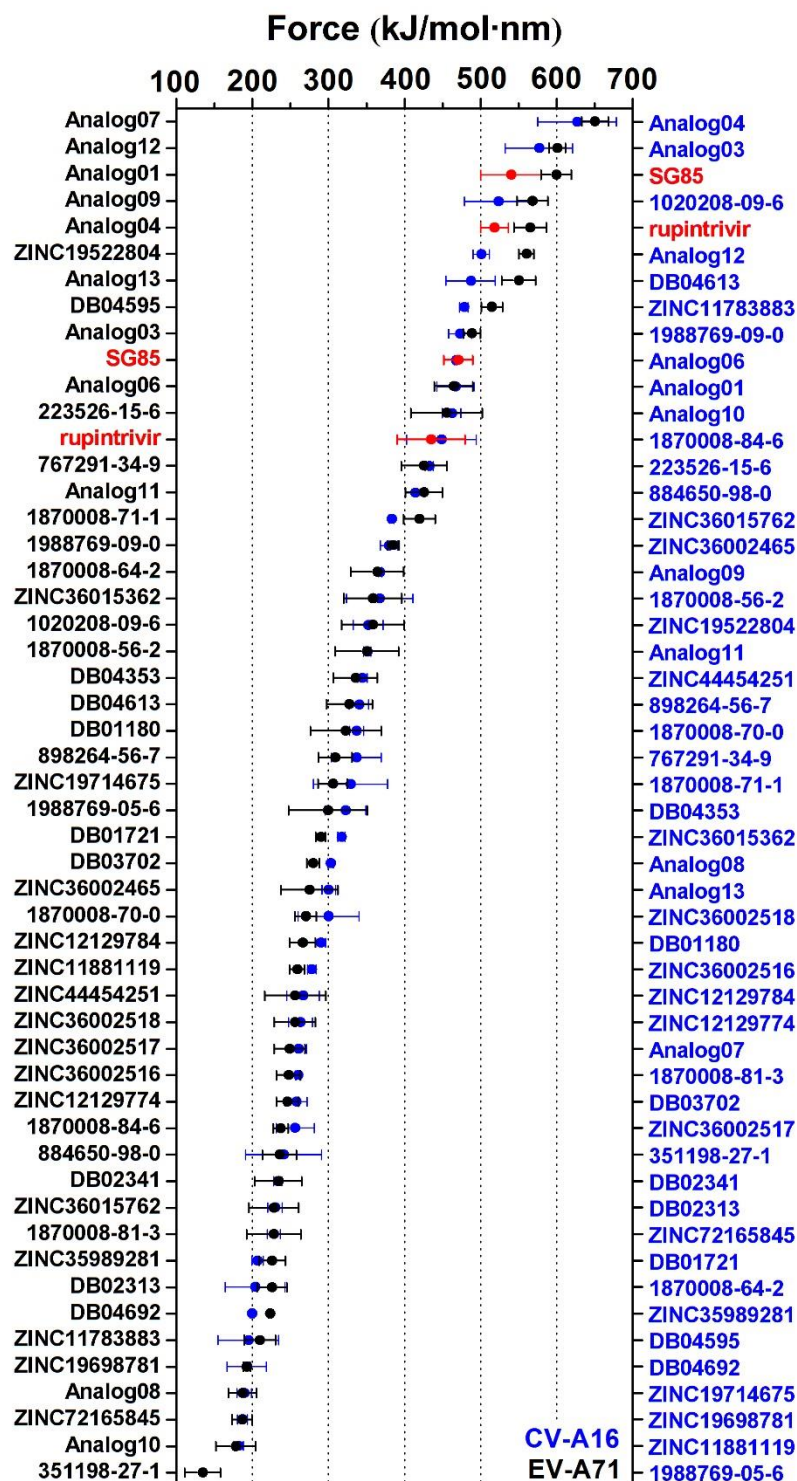
Figure 21 The rupture forces of the 52 ligands from SMD simulation approach with 3C^{pro} of CV-A16 and EV-A71. The vertical axis lists according to the rupture forces. Rupintrivir and SG85 are shown in red, whilst in blue are the ligands that are in complex with CV-A16 and black for EV-A71.
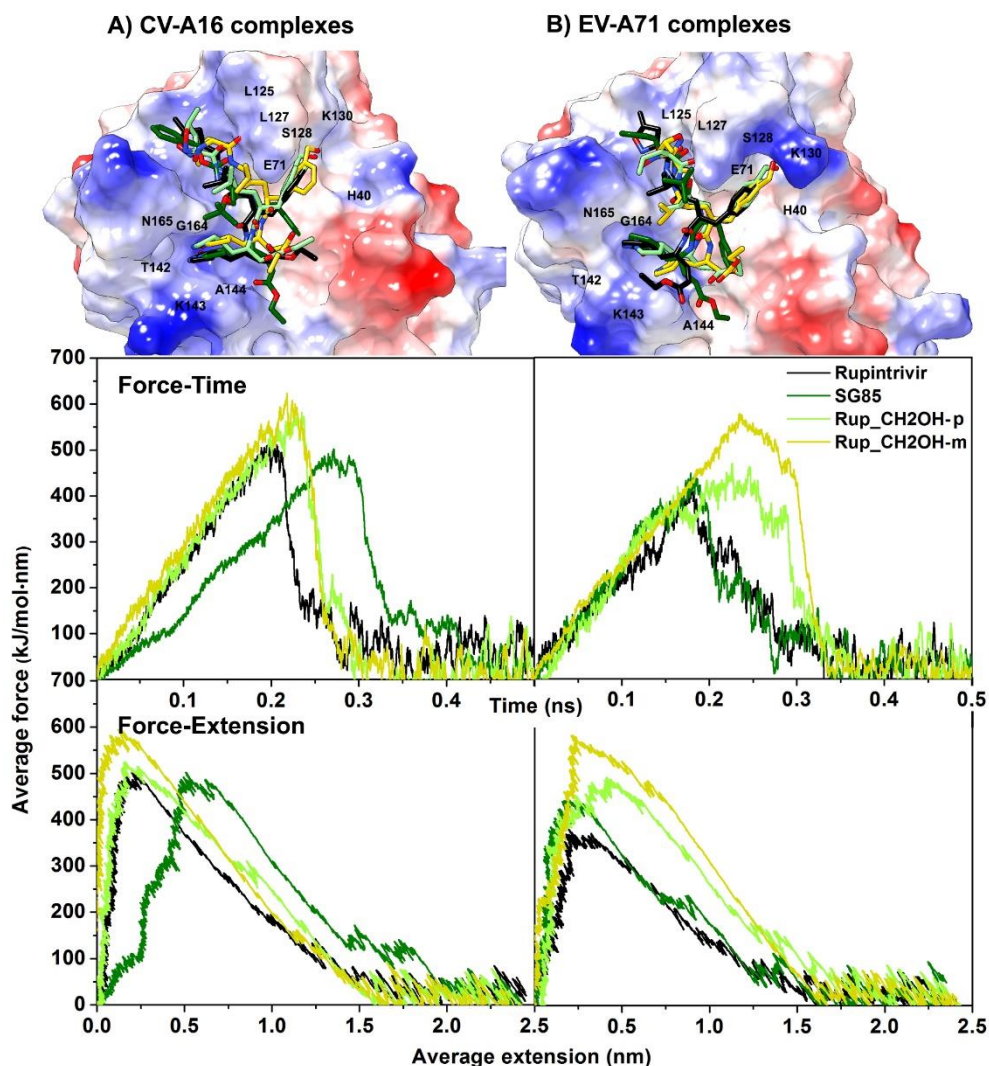
Figure 22 The superimposition of the best three candidate of screened compounds (Analog04, Analog03) in 3C^{pro} of CV-A16 and EV-A71 complexes are compared with rupintrivir and SG85 complexes. These values represent the maximum averaged rupture force of each system from each trajectory. The yellow represents analog04, light green shows analog03, dark green is SG85, and black denotes rupintrivir.

To clarify the top ranking of SMD screening, there are two metrics to test the force required for pulling; rupture force per time and the rupture force per extension. Rupintrivr appears to be released at around 0.2 nm from the docked location. The rupintrivir analogues in the EV-A71 system sustain interactions for a longer time than in the CV-A16 system (Figure 22). SG85 sustains interactions for a long time before releases from CV-A16, yet curiously not as much force is needed as one would expect.

Because of this, we should consider other compounds as being more potent inhibitors than SG85 if they can sustain long interactions and also stronger interactions.
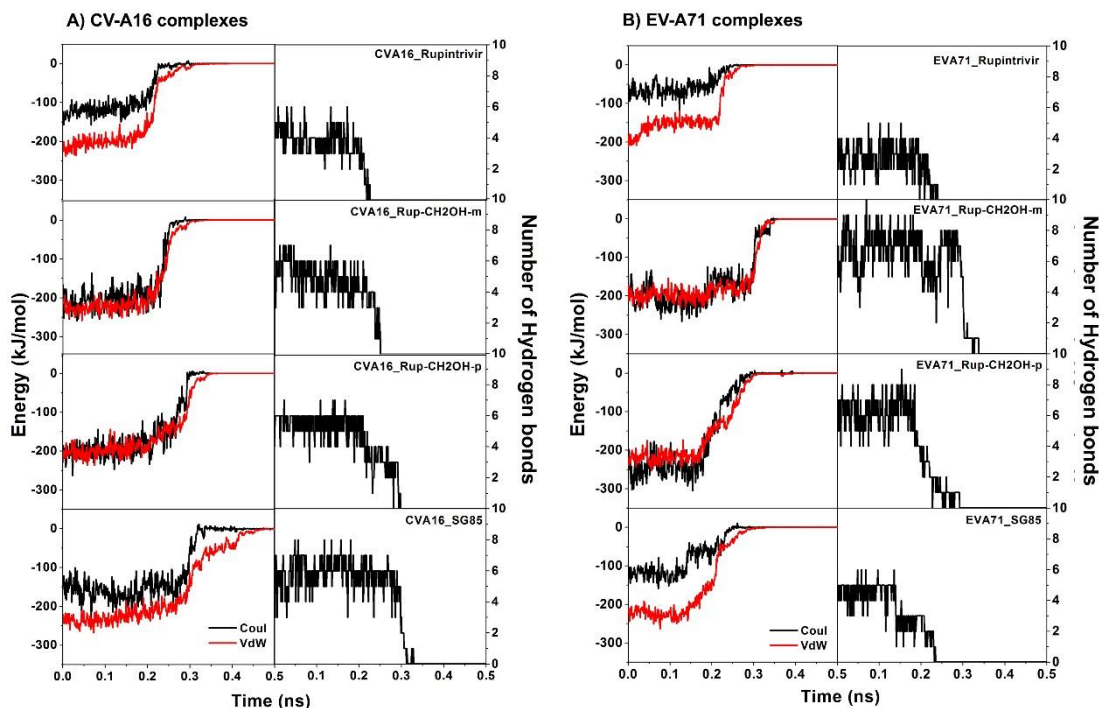
Figure 23 An analysis of the energetic bonding between A) CV-A16 and B) EV-A71 in complex with the rupintrivir, analog03, analog04, and SG85 ligands. The hydrogen bond analysis is shown in the sub-plots on the right. For the sub-plots on the left the electrostatic energy is shown in black and van der Waals energetics in red.

Rupintrivir and SG85 of both protease are strong vdW interaction energy [97]. We reiterate those findings when studying the specific types of interactions between the ligands and the 3C^{pro} variants (Figure 23). Every complex exhibits strong vdW interactions, especially in the rupintrivir analogs and SG85 (~200 kJ/mol). Hydrogen bonding enables prolonged binding of the complex hence analog04 can remain bonded the longest (Figure 22) due to having the highest number of hydrogen bonds between the protein and ligand (Figure 23).

4.2.4 The releasing analysis of inhibitor structure

The unbound state between inhibitor and 3C^{pro} can indicate the important residues that the keeping long interaction time mean the good ability of binding between atom of inhibitor and residue. From our previous findings [97], the important

residues for predicting involvement of hydrogen bonding between 3C^{pro} and a ligand are T142, G164, and S128. Herein we found that T142 and S128 were below the distance threshold of 3.5 Å except in the case of SG85 in complex with the 3C^{pro} of CV-A16.

In EV-A71 3C^{pro} analog04 (Figure 24B), the most strongly bound complex from the SMD simulations, had a distance of T142 backbone with P1-site of compound around 5 Å, implying hydrogen bond is not happening at this site. On the other hand, the energy deficit from the lack of hydrogen bond at the T142 site is compensated for by the H161 strongly binding at the P1-site of the ligand, which is released at around 0.300 ns, after the release of the P2-site of the ligand which is released around 0.290 ns and the P4-site around 0.280 ns, that represent the long time to keep interaction is slowing releasing, in the case of the EV-A71 variant. When comparing the same ligand with the CV-A16 complex, we found one crystal water molecule between G164 and T142 that possibly maintains the interaction with the -meta rupintrivir analog at the P1-site.

Analog03 of CV-A16 and EV-A71 are two complexes (Figure 24C) that have similar molecular dynamic characteristics. The P4-site is the last one to release in both cases, but EV-A71 3C^{pro} releases slightly later than the CV-A16 3C^{pro} in order to maintain a shorter distance. There are nothing to occur water molecule still in site between residues or ligand.

In the case of SG85 (Figure 24D) binding occurs near the C147 at the P2-site which is unique compared to the other complexes. The P2-site is the last site to leave from the receptor in EV-A71. In CV-A16, the last site is the P1-site which maintains in range until 0.268 ns.

In both variants of rupintrivir (Figure 24A), there was one crystal water molecule at the P1-site and the distance was more than 3.5 Å at 0.218 ns (CV-A16) and 0.220 ns (EV-A71). A notable point is that S128 in both complexes were pulled out from receptor that related with rupture force of CV-A16 being greater than that of the EV-A71 complex at 0.245 ns and 0.215 ns, respectively (Table 3).

Table 3 The time points at which each site of the ligand is no longer within 3.5 Å of the 3C^{pro} which approximates when the inhibitor is released from interacting with the protein. The measurements are taken at the P1'-site with G145, the P1-site with T142, the P2-site with E71, the P3-site with G164, and the P4-site and S128.

Sites	Time (ns)							
	CV-A16				EV-A71			
	Rupintrivir	Analog04	Analog03	SG85	Rupintrivir	Analog04	Analog03	SG85
P1'	0	0	0	0.27	0	0	0	0.02
P1	0.22	**0.24**	**0.23**	**0.29**	0.22	**0.30**	0.28	0.19
P2	0.21	**0.24**	0.19	0.24	0	0.29	0.28	0.20
P3	0.22	0.22	0.21	0.26	**0.22**	**0.30**	0.25	**0.21**
P4	**0.24**	**0.24**	0.22	0.24	0.21	0.22	**0.30**	0.14

The table 3 represent time of inhibitor releasing that based on hydrogen bond criteria (3.5 Å). In row, each sites of inhibitor are related with time at unbound state of EV-A71 and CV-A16. From my point of view, we suggest about site chain for additionally modify in the further at P1', P2 in EV-A71, and P3 in CV-A16 to increase the potential of binding between inhibitor and 3C^{pro}. In column, each structure were show number of site that keep interaction long time, the bold numbers are highest time of column. Analog04 in both CV-A16 and EV-A71 of 3C^{pro} could keep within the distance threshold longer time than other compounds at three-sites of the inhibitor (Table 3). This exposure displayed that analog04 could be assumed to predict a good effective inhibitor because of the strong interactions occurring between residue and inhibitor at these three binding sites in protease of CV-A16 and two sites in protease of EV-A71. The residues, S128, T142 and G145, were maintained a close proximity to the ligands up until the ultimate release, more so than other sites (Figure 24). According to Figure 24, the residues were kept distance between residues and inhibitor in long time that is T142, E71, and especially to S128. While, the E71 residue lack interaction with SG85 in EV-A71 and CV-A16. However, the both 3C^{pro} are able to replace interaction by C147 using pi-pi bond.
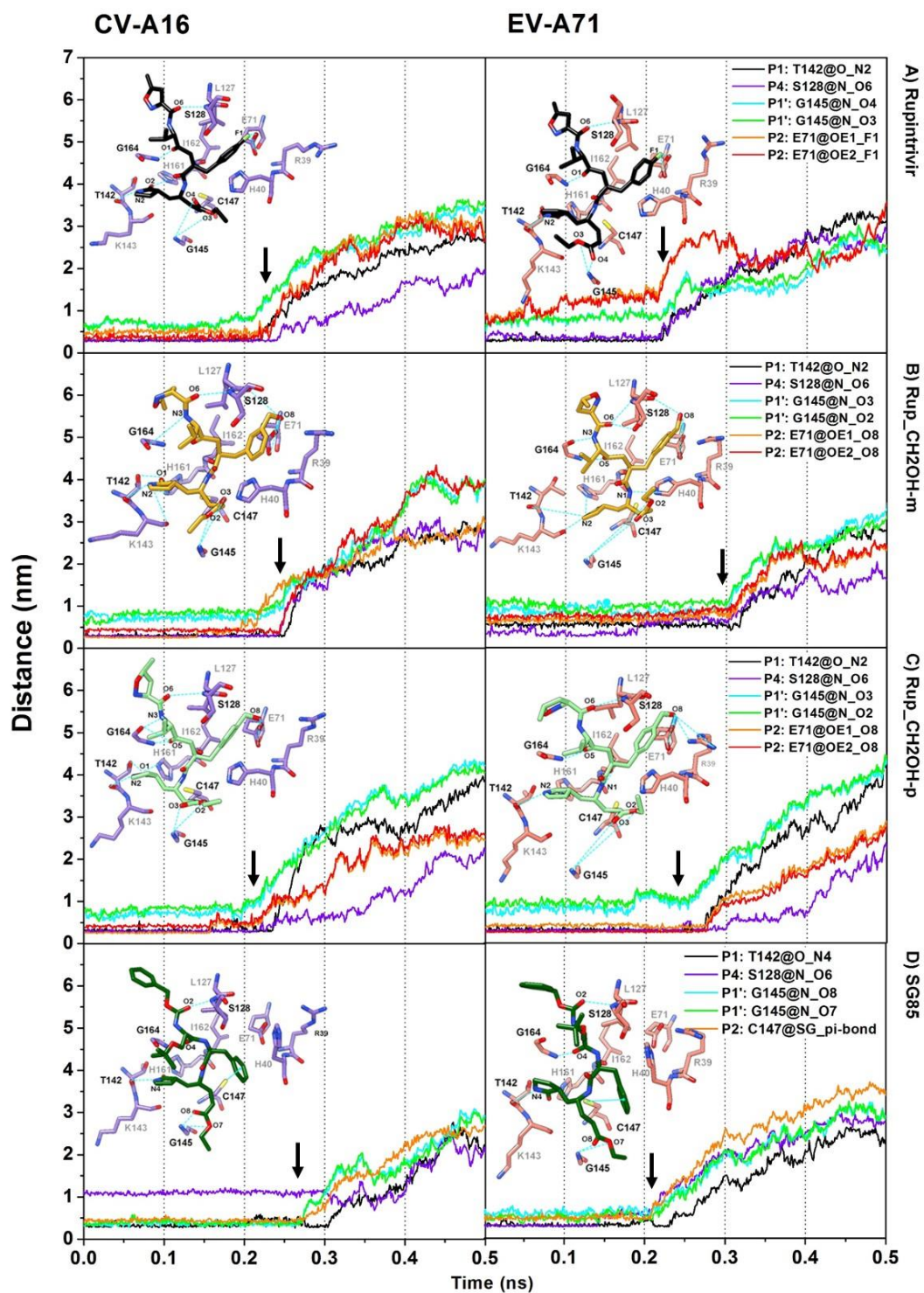
Figure 24 The atomic distances during pulling between residues and candidate inhibitors. On the vertical axis in each ligand case is distance, and on the horizontal axis is time. The purple color for 3C^{pro} of CV-A16 and pink for 3C^{pro} of EV-A71. Each

ligand   represent   using   difference   color;   Rupintrivir/black,   analog04/yellow, analog03/light green, SG85/dark green.

CHAPTER V:

CONCLUSIONS

5.1 The key binding study

Both inhibitors, rupintrivir and SG85, have very similar binding pattern to the 3C proteases of CV-A16, EV-A71 and EV-D68, which can be seen from the comparison of the crystal structures and from the per-residue decomposition free energies. From classical MD simulations, it is indicated that SG85 binds in a somewhat better way to CV-A16 and EV-D68 which are documented by hydrogen bond analyses and the calculation of the total binding free energy. On the contrary, for EV-A71 the affinities of both inhibitors are rather comparable. In this report, it is suggested that the SG85/CV-A16 and SG85/EV-D68 complexes are most convenient to describe the block of 3C^{pro} and can be used to develop further inhibitors of hand foot and mouth disease.

5.2 Visual screening

The SMD technique was applied to screen for potential HFMD agents from the ZINC database, DrugBank database, Scifinder database and ChemBL database repository along with several modified analogues of rupintrivir. Based on the hypothesis that a high required rupture force for pulling the ligand out of the CV-A16 binding site relates to a high predicted binding affinity and thereby inhibition efficiency. Several compounds were shown to have higher simulated binding efficacies than that of rupintrivir. To validate the method, the three known HFMD inhibitors (SG75, SG85 and SG98) were subjected to the same SMD analyses, where the derived F_{avg} values were found to be in good agreement with the experimental EC$_{50}$ values. According to the ranked F_{avg} of the 52 top-hit compounds obtained from the databases and structurally modified compounds based on rupintrivir, the analog04 and analog03 were suggested to have a better inhibitory affinity than rupintrivir and SG85. In addition to the predicted binding affinities derived from the theoretically obtained F_{avg} values,

the vdW interaction was found to show a higher contribution towards stabilizing the ligand in the active site of CV-A16 and EV-A71 3C^{pro} rather than electrostatic interaction.

Moreover, we suggest to modified functional group at P1' and P3 of each ligand for CV-A16, while P1' and P2 of each ligand for EV-A71, that possible to keep interaction with 3C^{pro} more.

Here we have shown that the two modifications of rupintrivir, analog04 and analog03, have higher simulated binding affinities than rupintrivir and SG85 themselves and suggest that these compounds be further investigated for *in vitro* and *in vivo* efficacy and inhibition against 3C^{pro} EV-A71 and CV-A16 ultimately with the goal of developing an anti-HFMD treatment.

REFERENCES

1. Lu, G., et al., *Enterovirus 71 and coxsackievirus A16 3C proteases: binding to rupintrivir and their substrates and anti-hand, foot, and mouth disease virus drug design.* J Virol, 2011. **85**(19): p. 10319-31.

2. Wang, J., et al., *Crystal Structures of Enterovirus 71 3C Protease Complexed with Rupintrivir Reveal the Roles of Catalytically Important Residues.* Journal of Virology, 2011. **85**(19): p. 10021-10030.

3. Lacroix, C., et al., *The Enterovirus 3C Protease Inhibitor SG85 Efficiently Blocks Rhinovirus Replication and Is Not Cross-Resistant with Rupintrivir.* Antimicrobial Agents and Chemotherapy, 2015. **59**(9): p. 5814-5818.

4. Zhou, H., et al., *Clinical characteristics of hand, foot and mouth disease in Harbin and the prediction of severe cases.* Chinese medical journal, 2012. **125**(7): p. 1261-1265.

5. Sarma, N., *Hand, foot, and mouth disease: current scenario and Indian perspective.* Indian J Dermatol Venereol Leprol, 2013. **79**(2): p. 165-75.

6. Gregory L. Repass, W.C.P., Fernando F. Stancampiano, *Hand, foot, and mouth disease: Identifying and managing an acute viral syndrome.* cleveland clinic journal of medicine, 2014. **81**(9): p. 7.

7. Samphutthanon, R., et al., *Spatio-Temporal Distribution and Hotspots of Hand, Foot and Mouth Disease (HFMD) in Northern Thailand.* International Journal of Environmental Research and Public Health, 2014. **11**(1): p. 312-336.

8. Huang, K.Y., et al., *Enterovirus 71 in Taiwan, 2004-2006: epidemiological and virological features.* Scand J Infect Dis, 2008. **40**(6-7): p. 571-4.

9. Chan, K.P., et al., *Epidemic hand, foot and mouth disease caused by human enterovirus 71, Singapore.* Emerg Infect Dis, 2003. **9**(1): p. 78-85.

10. AbuBakar, S., et al., *Identification of enterovirus 71 isolates from an outbreak of hand, foot and mouth disease (HFMD) with fatal cases of encephalomyelitis in Malaysia.* Virus Res, 1999. **61**(1): p. 1-9.

11. Thoa le, P.K., et al., *Genetic and antigenic characterization of enterovirus 71 in Ho Chi Minh City, Vietnam, 2011.* PLoS One, 2013. **8**(7): p. e69895.

12. Sabanathan, S., et al., *Enterovirus 71 related severe hand, foot and mouth disease outbreaks in South-East Asia: current situation and ongoing challenges.* Journal of Epidemiology and Community Health, 2014.

13. Dragovich, P.S., et al., *Structure-based design of irreversible, tripeptidyl human rhinovirus 3C protease inhibitors containing N-methyl amino acids.* Bioorganic & Medicinal Chemistry Letters, 1999. **9**(15): p. 2189-2194.

14. Zhu, R.N., et al., *[Study on the association of hand, foot and mouth disease and enterovirus 71/CA16 among children in Beijing, 2007].* Zhonghua Liu Xing Bing Xue Za Zhi, 2007. **28**(10): p. 1004-8.

15. Zhang, Y., et al., *An outbreak of hand, foot, and mouth disease associated with subgenotype C4 of human enterovirus 71 in Shandong, China.* J Clin Virol, 2009. **44**(4): p. 262-7.

16. Zhang, Y., et al., *An emerging recombinant human enterovirus 71 responsible for the 2008 outbreak of hand foot and mouth disease in Fuyang city of China.* Virol J, 2010. **7**: p. 94.

17. Tan, X., et al., *The Persistent Circulation of Enterovirus 71 in People's Republic of China: Causing Emerging Nationwide Epidemics Since 2008.* PLoS ONE, 2011. **6**(9): p. e25662.

18. Zhang, Y., et al., *Emergence and Transmission Pathways of Rapidly Evolving Evolutionary Branch C4a Strains of Human Enterovirus 71 in the Central Plain of China.* PLoS ONE, 2011. **6**(11): p. e27895.

19. Linsuwanon, P., et al., *The Fecal Virome of Children with Hand, Foot, and Mouth Disease that Tested PCR Negative for Pathogenic Enteroviruses.* PLoS ONE, 2015. **10**(8): p. e0135573.

20. Long, L., et al., *Neurological complications and risk factors of cardiopulmonary failure of EV-A71-related hand, foot and mouth disease.* Scientific Reports, 2016. **6**: p. 23444.

21.	da Silva, E.E., M.T. Winkler, and M.A. Pallansch, *Role of enterovirus 71 in acute flaccid paralysis after the eradication of poliovirus in Brazil.* Emerging Infectious Diseases, 1996. **2**(3): p. 231-233.

22.	Tan, C.W., et al., *Recent developments in antiviral agents against enterovirus 71 infection.* Journal of Biomedical Science, 2014. **21**(1): p. 14.

23.	Didier Hober, et al., *Viruses and Type 1 Diabetes: Focus on the Enteroviruses*, in *Type 1 Diabetes*, A. Escher, Editor. 2013: InTech.

24.	Andino, R., et al., *Intracellular determinants of picornavirus replication.* Trends in Microbiology, 1999. **7**(2): p. 76-82.

25.	Knipe DM, H.P., ed. *Picornaviridae: The Virus ans Their Repliation*. 5th ed., ed. R. VR. 2007. 796-839.

26.	Zhang, X.N., et al., *Rupintrivir is a promising candidate for treating severe cases of Enterovirus-71 infection.* World Journal of Gastroenterology, 2010. **16**(2): p. 201-209.

27.	Tan, J., et al., *3C Protease of Enterovirus 68: Structure-Based Design of Michael Acceptor Inhibitors and Their Broad-Spectrum Antiviral Effects against Picornaviruses.* Journal of Virology, 2013. **87**(8): p. 4339-4351.

28.	Smee, D.F., et al., *Susceptibilities of enterovirus D68, enterovirus 71, and rhinovirus 87 strains to various antiviral compounds.* Antiviral Research, 2016. **131**: p. 61-65.

29.	Binford, S.L., et al., *Conservation of amino acids in human rhinovirus 3C protease correlates with broad-spectrum antiviral activity of rupintrivir, a novel human rhinovirus 3C protease inhibitor.* Antimicrobial Agents and Chemotherapy, 2005. **49**(2): p. 619-626.

30.	Matthews, D.A., et al., *Structure-assisted design of mechanism-based irreversible inhibitors of human rhinovirus 3C protease with potent antiviral activity against multiple rhinovirus serotypes.* Proc Natl Acad Sci U S A, 1999. **96**(20): p. 11000-7.

31.	Patick, A.K., et al., *In vitro antiviral activity of AG7088, a potent inhibitor of human rhinovirus 3C protease.* Antimicrob Agents Chemother, 1999. **43**(10): p. 2444-50.

32.   Patick, A.K., *Rhinovirus chemotherapy.* Antiviral Research, 2006. **71**(2-3): p. 391-396.

33.   Zhang, X., et al., *Rupintrivir is a promising candidate for treating severe cases of enterovirus-71 infection: Evaluation of antiviral efficacy in a murine infection model.* Antiviral Research, 2013. **97**(3): p. 264-269.

34.   Binford, S.L., et al., *In vitro resistance study of rupintrivir, a novel inhibitor of human rhinovirus 3C protease.* Antimicrob Agents Chemother, 2007. **51**(12): p. 4366-73.

35.   Ooi, M.H., et al., *Clinical features, diagnosis, and management of enterovirus 71.* Lancet Neurol, 2010. **9**(11): p. 1097-105.

36.   Sun, L., et al., *Antiviral activity of broad-spectrum and enterovirus-specific inhibitors against clinical isolates of enterovirus D68.* Antimicrob Agents Chemother, 2015.

37.   Hayden, F.G., et al., *Phase II, randomized, double-blind, placebo-controlled studies of ruprintrivir nasal spray 2-percent suspension for prevention and treatment of experimentally induced rhinovirus colds in healthy volunteers.* Antimicrob Agents Chemother, 2003. **47**(12): p. 3907-16.

38.   Lee, J.C., et al., *A mammalian cell-based reverse two-hybrid system for functional analysis of 3C viral protease of human enterovirus 71.* Anal Biochem, 2008. **375**(1): p. 115-23.

39.   Tsai, M.-T., et al., *Real-Time Monitoring of Human Enterovirus (HEV)-Infected Cells and Anti-HEV 3C Protease Potency by Fluorescence Resonance Energy Transfer.* Antimicrobial Agents and Chemotherapy, 2009. **53**(2): p. 748-755.

40.   Morris, G.M. and M. Lim-Wilby, *Molecular Docking*, in *Molecular Modeling of Proteins*, A. Kukol, Editor. 2008, Humana Press: Totowa, NJ. p. 365-382.

41.   Mustard, D. and D.W. Ritchie, *Docking essential dynamics eigenstructures.* Proteins: Structure, Function, and Bioinformatics, 2005. **60**(2): p. 269-274.

42.   Wu, G., et al., *Detailed analysis of grid-based molecular docking: A case study of CDOCKER-A CHARMm-based MD docking algorithm.* J Comput Chem, 2003. **24**(13): p. 1549-62.

43.   Vieth, M. and D.J. Cummins, *DoMCoSAR: A Novel Approach for Establishing the Docking Mode That Is Consistent with the Structure–Activity Relationship. Application to HIV-1 Protease Inhibitors and VEGF Receptor Tyrosine Kinase Inhibitors.* Journal of Medicinal Chemistry, 2000. **43**(16): p. 3020-3032.

44.   Vieth, M., et al., *Assessing energy functions for flexible docking.* Journal of Computational Chemistry, 1998. **19**(14): p. 1612-1622.

45.   Tirado-Rives, J. and W.L. Jorgensen, *Contribution of Conformer Focusing to the Uncertainty in Predicting Free Energies for Protein–Ligand Binding.* Journal of Medicinal Chemistry, 2006. **49**(20): p. 5880-5884.

46.   Shoichet, B., et al., *Structure-based discovery of inhibitors of thymidylate synthase.* Science, 1993. **259**(5100): p. 1445-1450.

47.   McGann, M.R., et al., *Gaussian docking functions.* Biopolymers, 2003. **68**(1): p. 76-90.

48.   Jones, G., et al., *Development and validation of a genetic algorithm for flexible docking1.* Journal of Molecular Biology, 1997. **267**(3): p. 727-748.

49.   Goodsell, D.S., G.M. Morris, and A.J. Olson, *Automated docking of flexible ligands: Applications of autodock.* Journal of Molecular Recognition, 1996. **9**(1): p. 1-5.

50.   Bahar, I., A.R. Atilgan, and B. Erman, *Direct evaluation of thermal fluctuations in proteins using a single-parameter harmonic potential.* Folding and Design, 1997. **2**(3): p. 173-181.

51.   Boas, F.E. and P.B. Harbury, *Potential energy functions for protein design.* Current Opinion in Structural Biology, 2007. **17**(2): p. 199-204.

52.   Shattuck, T.W. *Molecular Mechanics Tutorial 2008*. September,2008, 2008. 77.

53.   Marcus Hennecke, R.M., Herb Swan. *Parameter Files*. [cited 2016 27-Oct]; Available from: http://www.ks.uiuc.edu/Training/Tutorials/namd/namd-tutorial-win-html/node26.html#bondstretch.

54.   MacKerell, A.D., et al., *All-Atom Empirical Potential for Molecular Modeling and Dynamics Studies of Proteins.* The Journal of Physical Chemistry B, 1998. **102**(18): p. 3586-3616.

55.   Ha, S.N., et al., *A revised potential-energy surface for molecular mechanics studies of carbohydrates.* Carbohydrate Research, 1988. **180**(2): p. 207-221.

56.   Schlenkrich, M., et al., *An Empirical Potential Energy Function for Phospholipids: Criteria for Parameter Optimization and Applications*, in *Biological Membranes: A Molecular Perspective from Computation and Experiment*, K.M. Merz and B. Roux, Editors. 1996, Birkhäuser Boston: Boston, MA. p. 31-81.

57.   MacKerell, A.D., J. Wiorkiewicz-Kuczera, and M. Karplus, *An all-atom empirical energy function for the simulation of nucleic acids.* Journal of the American Chemical Society, 1995. **117**(48): p. 11946-11975.

58.   M. Nic and B.K. J. Jirat, *Compendium of Chemical Terminology*, ed. 2nd. 1997: Blackwell Scientific Publications.

59.   Galina L. KLIMCHITSKAYA and V.M. MOSTEPANENKO, *CASIMIR AND VAN DER WAALS FORCES: ADVANCES AND PROBLEMS.* BASIC RESEARCH IN PHYSICS, 2015. **517**(1): p. 41-65.

60.   Larcombe, L., *Molecular modelling for in silico drug discovery*. 2014.

61.   Okumura, H., *Molecular dynamics simulation and temperature replica-exchange method*. 2014, Institute for Molecular Science, Japan.

62.   Suan Li, M. and B. Khanh Mai, *Steered Molecular Dynamics-A Promising Tool for Drug Design.* Current Bioinformatics, 2012. **7**(4): p. 342-351.

63.   Isralewitz, B., M. Gao, and K. Schulten, *Steered molecular dynamics and mechanical functions of proteins.* Current Opinion in Structural Biology, 2001. **11**(2): p. 224-230.

64.   Strzelecki, J., et al. *AFM force spectroscopy and steered molecular dynamics simulation of protein contactin 4*. in *Acta Physica Polonica A*. 2009. Polish Academy of Sciences Warsaw.

65.   Honig, B. and A. Nicholls, *Classical electrostatics in biology and chemistry.* Science, 1995. **268**(5214): p. 1144-9.

66.   Lu, Q. and R. Luo, *A Poisson–Boltzmann dynamics method with nonperiodic boundary condition.* The Journal of Chemical Physics, 2003. **119**(21): p. 11035-11047.

67.   Wang, J. and R. Luo, *Assessment of linear finite-difference Poisson-Boltzmann solvers.* J Comput Chem, 2010. **31**(8): p. 1689-98.

68.   Cai, Q., et al., *Performance of Nonlinear Finite-Difference Poisson–Boltzmann Solvers.* Journal of Chemical Theory and Computation, 2010. **6**(1): p. 203-211.

69.   Weiser, J., P.S. Shenkin, and W.C. Still, *Approximate atomic surfaces from linear combinations of pairwise overlaps (LCPO).* Journal of Computational Chemistry, 1999. **20**(2): p. 217-230.

70.   Srinivasan, J., et al., *Application of a pairwise generalized Born model to proteins and nucleic acids: inclusion of salt effects.* Theoretical Chemistry Accounts, 1999. **101**(6): p. 426-434.

71.   Olsson, M.H., Chresten R. Søndergaard, Michal Rostkowski, and Jan H. Jensen., *PROPKA3: consistent treatment of internal and surface residues in empirical pKa predictions.* Journal of Chemical Theory and Computation, 2011. **7**(2): p. 12.

72.   Sangpheak, W., et al., *Enhanced stability of a naringenin/2,6-dimethyl beta-cyclodextrin inclusion complex: molecular dynamics and free energy calculations based on MM- and QM-PBSA/GBSA.* J Mol Graph Model, 2014. **50**: p. 10-5.

73.   Nutho, B., et al., *Binding mode and free energy prediction of fisetin/β-cyclodextrin inclusion complexes.* Beilstein Journal of Organic Chemistry, 2014. **10**: p. 2789-2799.

74.   Meeprasert, A., et al., *In silico screening for potent inhibitors against the NS3/4A protease of hepatitis C virus.* Curr Pharm Des, 2014. **20**(21): p. 3465-77.

75.   Frisch, M.J., et al., *Gaussian 09*. 2009, Gaussian, Inc.: Wallingford, CT, USA.

76.   Duan, Y., et al., *A point-charge force field for molecular mechanics simulations of proteins based on condensed-phase quantum mechanical calculations.* J Comput Chem, 2003. **24**(16): p. 1999-2012.

77.   Wang, J., Wolf, R. M.; Caldwell, J. W.;Kollman, P. A.; Case, D. A., *Development and testing of a general AMBER force field.* Journal of Computational Chemistry, 2004. **25**: p. 17.

78.   Wang, J., Wang, W., Kollman P. A.; Case, D. A. , *Automatic atom type and bond type perception in molecular mechanical calculations.* Journal of Molecular Graphics and Modelling, 2006. **25**: p. 13.

79.   Irwin, J.J., et al., *ZINC: A Free Tool to Discover Chemistry for Biology.* Journal of Chemical Information and Modeling, 2012. **52**(7): p. 1757-1768.

80.   Wishart, D.S., et al., *DrugBank: a comprehensive resource for in silico drug discovery and exploration.* Nucleic Acids Res, 2006. **34**(Database issue): p. D668-72.

81.   Willighagen, E.L., et al., *The ChEMBL database as linked open data.* Journal of Cheminformatics, 2013. **5**: p. 23-23.

82.   Scholar, S. *Chemical Abstracts Service: Columbus*. 2004   [cited 2016 12Sep,2016]; RN 133876-92-3].

83.   Schrodinger, LLC, *The PyMOL Molecular Graphics System, Version 1.3r1*. 2010.

84.   Wang, J., et al., *Automatic atom type and bond type perception in molecular mechanical calculations.* Journal of Molecular Graphics and Modelling, 2006. **25**(2): p. 247-260.

85.   Wang, J., et al., *Development and testing of a general amber force field.* J Comput Chem, 2004. **25**(9): p. 1157-74.

86.   D.A. Case, V.B., J.T. Berryman, R.M. Betz, Q. Cai, D.S. Cerutti, T.E. Cheatham, III, T.A. Darden, R.E., et al., *AMBER 14*. 2014, University of California, San Francisco.

87.   Sousa da Silva, A.W. and W.F. Vranken, *ACPYPE - AnteChamber PYthon Parser interfacE.* BMC Research Notes, 2012. **5**: p. 367-367.

88.   Jorgensen, W.L., et al., *Comparison of simple potential functions for simulating liquid water.* The Journal of Chemical Physics, 1983. **79**(2): p. 926-935.

89.   Meeprasert, A., S. Hannongbua, and T. Rungrotmongkol, *Key Binding and Susceptibility of NS3/4A Serine Protease Inhibitors against Hepatitis C Virus.* Journal of Chemical Information and Modeling, 2014. **54**(4): p. 1208-1217.

90.   Kaiyawet, N., T. Rungrotmongkol, and S. Hannongbua, *Effect of Halogen Substitutions on dUMP to Stability of Thymidylate Synthase/dUMP/mTHF Ternary Complex Using Molecular Dynamics Simulation.* Journal of Chemical Information and Modeling, 2013. **53**(6): p. 1315-1323.

91.   Nunthaboot, N., et al., *Molecular insights into human receptor binding to 2009 H1N1 influenza A hemagglutinin.* Monatshefte für Chemie - Chemical Monthly, 2010. **141**(7): p. 801-807.

92.   Salomon-Ferrer, R., et al., *Routine Microsecond Molecular Dynamics Simulations with AMBER on GPUs. 2. Explicit Solvent Particle Mesh Ewald.* Journal of Chemical Theory and Computation, 2013. **9**(9): p. 3878-3888.

93.   York, D.M., T.A. Darden, and L.G. Pedersen, *The effect of long‐range electrostatic interactions in simulations of macromolecular crystals: A comparison of the Ewald and truncated list methods.* The Journal of Chemical Physics, 1993. **99**(10): p. 8345-8348.

94.   Roe, D.R. and T.E. Cheatham, *PTRAJ and CPPTRAJ: Software for Processing and Analysis of Molecular Dynamics Trajectory Data.* Journal of Chemical Theory and Computation, 2013. **9**(7): p. 3084-3095.

95.   Hess, B., et al., *GROMACS 4: Algorithms for Highly Efficient, Load-Balanced, and Scalable Molecular Simulation.* Journal of Chemical Theory and Computation, 2008. **4**(3): p. 435-447.

96.   Wang, J., et al., *Development and testing of a general amber force field.* Journal of Computational Chemistry, 2004. **25**(9): p. 1157-1174.

97.   Jetsadawisut, W., et al., *Susceptibility of inhibitors against 3C protease of coxsackievirus A16 and enterovirus A71 causing hand, foot and mouth disease: A molecular dynamics study.* Biophysical Chemistry, 2016. **219**: p. 9-16.

98.   Bjelkmar, P., et al., *Implementation of the CHARMM Force Field in GROMACS: Analysis of Protein Stability Effects from Correction Maps, Virtual Interaction Sites, and Water Models.* Journal of Chemical Theory and Computation, 2010. **6**(2): p. 459-466.

99.   Abraham, M.J. and J.E. Gready, *Optimization of parameters for molecular dynamics simulation using smooth particle-mesh Ewald in GROMACS 4.5.* Journal of Computational Chemistry, 2011. **32**(9): p. 2031-2040.

100.   BIOVIA, D.S., *Discovery Studio Modeling Environment*, R. 2017, Editor. 2016: San Diego: Dassault Systèmes.

101. Wang, J., et al., *Crystal structures of enterovirus 71 3C protease complexed with rupintrivir reveal the roles of catalytically important residues.* J Virol, 2011. **85**.

102. Barbora Kozlíková, et al. *Analysis of Tunnels in Static and Dynamic Protein Structures*. 2013; Available from: http://caver.cz/index.php?sid=120.

103. Chovancova, E., et al., *CAVER 3.0: A Tool for the Analysis of Transport Pathways in Dynamic Protein Structures.* PLoS Comput Biol, 2012. **8**(10): p. e1002708.

104. Kozlikova, B., et al., *CAVER Analyst 1.0: graphic tool for interactive visualization and analysis of tunnels and channels in protein structures.* Bioinformatics, 2014.

105. Medek P., B.P., Sochor J, *Computation of tunnels in protein molecules using Delaunay triangulation.* Journal of WSCG, 2007. **15**(1-3): p. 7.

106. Team, C., *Protein tunnels*, in *png*, tunnel, Editor. 2015: Wikipedia EN. p. Redrawn by hand based on this file: File:ApproximateVoronoiDiagram.png (on Wikipedia EN, not on Commons). This file contains layers and other helpful information for Inkscape editor.

107. de Beer, T.A.P., et al., *PDBsum additions.* Nucleic Acids Research, 2014. **42**(Database issue): p. D292-D296.

108. Vuong, Q.V., T.T. Nguyen, and M.S. Li, *A New Method for Navigating Optimal Direction for Pulling Ligand from Binding Pocket: Application to Ranking Binding Affinity by Steered Molecular Dynamics.* Journal of Chemical Information and Modeling, 2015. **55**(12): p. 2731-2738.

109. Mai, B.K., M.H. Viet, and M.S. Li, *Top Leads for Swine Influenza A/H1N1 Virus Revealed by Steered Molecular Dynamics Approach.* Journal of Chemical Information and Modeling, 2010. **50**(12): p. 2236-2247.

110. Mai, B.K. and M.S. Li, *Neuraminidase inhibitor R-125489--a promising drug for treating influenza virus: steered molecular dynamics approach.* Biochem Biophys Res Commun, 2011. **410**(3): p. 688-91.

APPENDIX

VITA

--- PERSONAL DATA ---   --- EDUCATION ---

Name: Miss Warin Jetsadawisut   2014-present (M.Sc.) Department of chemistry,

Email: Warin.jetsadawisut@gmail.com   faculty of science, Chulalongkorn university

Nationality: Thai   2009-2013 (B.Sc.) Department of chemistry,

                                                          faculty of science, Chulalongkorn university,

                                                          2003-2008 Bodindecha (Sing Singhaseni) 2

--- EXPERIENCES ---

2016:

- Jetsadawisut W. et.al., (2016). In Silico Screening for Potent Anti-viral Agents Against Enterovirus

A71 and Coxsackievirus A16 3C proteases. (manuscript)

- Jetsadawisut W. et.al., (2016). Susceptibility of inhibitors against 3C protease of coxsackievirus A16

and enterovirus A71 causing hand, foot and mouth disease: A molecular dynamics study.

Biophysical Chemistry, 219, 9-16

- Oral presentation in The 20th International Annual Symposium on Computational Science

and Engineering (20th ANSCSE), Bangkok

- Short time research at University of Vienna, Austria

- Poster presentation in Pure and Applied Chemistry international conference 2016, Bangkok

- Poster presentation in 7th Asia-Pacific Conference of Theoretical and Computational

Chemistry, Taiwan

2015:

- Participant in Molecular Designs for Advanced Materials, Chiang Mai

2014:

- Poster presentation in Thai summer school of computational chemistry

2013:

- Oral presentation in The 18th International Annual Symposium on Computational Science

and Engineering (18th ANSCSE), Chonburi